



**HAL**  
open science

## Receptor dimerization dynamics as a regulatory valve for plasticity of type I interferon signaling.

Stephan Wilmes, Oliver Beutel, Zhi Li, Véronique François-Newton, Christian Richter, Dennis Janning, Cindy Kroll, Patrizia Hanhart, Katharina Hötte, Changjiang You, et al.

### ► To cite this version:

Stephan Wilmes, Oliver Beutel, Zhi Li, Véronique François-Newton, Christian Richter, et al.. Receptor dimerization dynamics as a regulatory valve for plasticity of type I interferon signaling.. *Journal of Cell Biology*, 2015, 209 (4), pp.579-593. 10.1083/jcb.201412049 . pasteur-02070629

**HAL Id: pasteur-02070629**

**<https://pasteur.hal.science/pasteur-02070629>**

Submitted on 18 Mar 2019

**HAL** is a multi-disciplinary open access archive for the deposit and dissemination of scientific research documents, whether they are published or not. The documents may come from teaching and research institutions in France or abroad, or from public or private research centers.

L'archive ouverte pluridisciplinaire **HAL**, est destinée au dépôt et à la diffusion de documents scientifiques de niveau recherche, publiés ou non, émanant des établissements d'enseignement et de recherche français ou étrangers, des laboratoires publics ou privés.



Distributed under a Creative Commons Attribution - ShareAlike 4.0 International License

# Receptor dimerization dynamics as a regulatory valve for plasticity of type I interferon signaling

Stephan Wilmes,<sup>1</sup> Oliver Beutel,<sup>1</sup> Zhi Li,<sup>2</sup> Véronique Francois-Newton,<sup>2</sup> Christian P. Richter,<sup>1</sup> Dennis Janning,<sup>1</sup> Cindy Kroll,<sup>1</sup> Patrizia Hanhart,<sup>1</sup> Katharina Hötte,<sup>1</sup> Changjiang You,<sup>1</sup> Gilles Uzé,<sup>3</sup> Sandra Pellegrini,<sup>2</sup> and Jacob Piehler<sup>1</sup>

<sup>1</sup>Department of Biology, Division of Biophysics, University of Osnabrück, 49074 Osnabrück, Germany

<sup>2</sup>Institut Pasteur, Cytokine Signaling Unit, Centre National de la Recherche Scientifique URA1961, 75724 Paris, France

<sup>3</sup>Centre National de la Recherche Scientifique Montpellier, 34095 Montpellier, France

**T**ype I interferons (IFNs) activate differential cellular responses through a shared cell surface receptor composed of the two subunits, IFNAR1 and IFNAR2. We propose here a mechanistic model for how IFN receptor plasticity is regulated on the level of receptor dimerization. Quantitative single-molecule imaging of receptor assembly in the plasma membrane of living cells clearly identified IFN-induced dimerization of IFNAR1 and IFNAR2. The negative feedback regulator ubiquitin-specific protease 18 (USP18) potentially interferes with the recruitment of IFNAR1

into the ternary complex, probably by impeding complex stabilization related to the associated Janus kinases. Thus, the responsiveness to IFN $\alpha$ 2 is potentially down-regulated after the first wave of gene induction, while IFN $\beta$ , due to its  $\sim$ 100-fold higher binding affinity, is still able to efficiently recruit IFNAR1. Consistent with functional data, this novel regulatory mechanism at the level of receptor assembly explains how signaling by IFN $\beta$  is maintained over longer times compared with IFN $\alpha$ 2 as a temporally encoded cause of functional receptor plasticity.

## Introduction

Functional plasticity, i.e., the ability to elicit differential cellular responses through the same cell surface receptor by means of different ligands, is a frequently observed feature of cytokine receptor signaling (Moraga et al., 2014), which plays an important role for drug development (Schreiber and Walter, 2010). The molecular mechanisms regulating functional plasticity have so far remained unclear, though some common determinants are emerging (Moraga et al., 2014). A prominent paradigm of cytokine receptor plasticity is the type I interferon (IFN) receptor. All 15 members of the human IFN family recruit a shared cell surface receptor comprising the subunits IFNAR1 and IFNAR2 (Uzé et al., 1992, 2007; Novick et al., 1994; Pestka et al., 2004), through which they activate a broad spectrum of defense mechanisms against pathogen infection and malignancy development (Deonarain et al., 2002; Parmar and Platanius, 2003; Decker et al., 2005; Hertzog and Williams, 2013; Schneider et al., 2014).

Differential cellular responses activated by different IFNs have been reported for numerous instances (Abramovich et al., 1994; Rani et al., 1996; Coelho et al., 2005; Uzé et al., 2007). Although all IFNs induce antiviral activity with very similar potencies, other cellular responses regulating proliferation and differentiation are much more potently induced by IFN $\beta$  compared with IFN $\alpha$  subtypes. Detailed mutational studies on the IFN–receptor interaction (Piehler and Schreiber, 1999b; Runkel et al., 2000; Roisman et al., 2001; Cajean-Feroldi et al., 2004; Lamken et al., 2005; Strunk et al., 2008), as well as extensive low- and high-resolution structural data on the binary and ternary complexes (Chill et al., 2003; Quadt-Akabayov et al., 2006; Li et al., 2008; Strunk et al., 2008; Thomas et al., 2011; de Weerd et al., 2013), clearly established that, rather than differences in the structure, the diverse binding affinities of IFNs toward the receptor subunits are responsible for differential signaling (Subramaniam et al., 1995; Russell-Harde et al., 1999; Lamken et al., 2004; Jaks et al., 2007; Lavoie et al., 2011). In particular, the  $\sim$ 100-fold higher binding affinity toward IFNAR1 observed for IFN $\beta$  compared with IFN $\alpha$  subtypes was suggested to be responsible

Correspondence to Jacob Piehler: [piehler@uos.de](mailto:piehler@uos.de)

Abbreviations used in this paper: HBS, HEPES-buffered saline; HTL, HaloTag ligand; IFN, type I interferon; IFNAR, type I interferon receptor; JAK, Janus kinase; MBP, maltose-binding protein; PEG, poly(ethylene glycol); PICCS, particle image cross-correlation spectroscopy; PLL, poly-L-lysine; STAT, signal transducer and activator of transcription; TIRFM, total internal reflection fluorescence microscopy; TMR, tetramethyl rhodamine; USP, ubiquitin-specific protease; wt, wild type.

© 2015 Wilmes et al. This article is distributed under the terms of an Attribution–Noncommercial–Share Alike–No Mirror Sites license for the first six months after the publication date [see <http://www.rupress.org/terms>]. After six months it is available under a Creative Commons License [Attribution–Noncommercial–Share Alike 3.0 Unported license, as described at <http://creativecommons.org/licenses/by-nc-sa/3.0/>].

for unique functions attributed to IFN $\beta$  (Domanski et al., 1998; Russell-Harde et al., 1999; Lamken et al., 2004). Strikingly, functional properties specific to IFN $\beta$  could be very well mimicked by IFN $\alpha$ 2 mutants with similar binding affinities toward IFNAR1 (Jaitin et al., 2006; Kalie et al., 2007). The critical role of the binding affinity toward IFNAR1 suggested that recruitment of this low-affinity receptor subunit into the signaling complex plays an important regulatory role in receptor plasticity (Piehler et al., 2012). Quantitative studies of IFN-induced receptor assembly on artificial membranes indeed suggested that, at physiological receptor concentrations in the plasma membrane (typically 0.1–1/ $\mu\text{m}^2$ ), receptor dimerization by IFN $\alpha$ 2 may be much less effective than by IFN $\beta$  (Lamken et al., 2004; Jaitin et al., 2006).

Recently, ubiquitin-specific protease 18 (USP18) was identified as a negative feedback regulator of IFN signaling (Malakhova et al., 2006), and was shown to be a key determinant for the differential activity of IFN $\alpha$ 2 and IFN $\beta$  (François-Newton et al., 2011; François-Newton et al., 2012). Interestingly, USP18 was found to interfere with IFN binding and uptake without significant alteration of the receptor density (François-Newton et al., 2011), probably acting via an interaction with the cytosolic domain of IFNAR2 (Malakhova et al., 2006; Löchte et al., 2014). This evidence suggests a potential regulatory mechanism of USP18 on the level of receptor assembly. Here, we aimed to pinpoint the mechanism of type I interferon receptor (IFNAR) assembly in living cells in a quantitative manner to define the role of IFNAR1 binding affinity as well as the regulatory function of USP18 for the formation of the ternary signaling complex. Because, according to the law of mass action, the receptor density determines the equilibrium between binary and ternary complex on the plasma membrane (Fig. 1 a), we established single-molecule imaging techniques that were able to monitor and quantify protein–protein interactions on the cell surface at physiological receptor expression levels. For probing dimerization of endogenous receptors, we used fluorescently labeled IFNs with engineered binding affinities as reporters. Moreover, using tagged versions of IFNAR1 and IFNAR2 expressed at physiological levels, we established quantitative single-molecule receptor dimerization assays based on dual-color single-molecule colocalization and colocomotion assays (Schütz et al., 1998; Koyama-Honda et al., 2005; Suzuki et al., 2007, 2012; Low-Nam et al., 2011). We unambiguously demonstrate IFN-induced dimerization of IFNAR1 and IFNAR2 and the limiting role of IFNAR1 binding affinity in complex assembly. Interestingly, the dynamic equilibrium between binary and ternary complexes is modulated by USP18, which appears to interfere with cytosolic stabilization likely mediated by the Janus kinases (JAKs). Based on these insights, we propose a model describing how IFN receptor plasticity is regulated at the level of receptor assembly.

## Results

### Single-molecule IFN binding and diffusion

To probe dimerization of endogenous IFNAR1 and IFNAR2, we developed an in situ IFN binding assay based on single-molecule fluorescence imaging. We have previously demonstrated that

the dissociation kinetics of IFNs can be taken as a measure for probing the equilibrium between binary and ternary complexes on artificial membranes (Lamken et al., 2004; Gavutis et al., 2005). The key concept is that IFN simultaneously interacting with IFNAR1 and IFNAR2 dissociates much slower than when interacting with IFNAR2 only. Thus, the effective cell surface binding affinity of IFN $\alpha$ 2 to cells expressing IFNAR1 and IFNAR2 is typically 10–20-fold higher ( $K_d = \sim 200$  pM) compared with the interaction with IFNAR2 only ( $K_d = \sim 3$  nM, see [Table S1](#); Cohen et al., 1995; Moraga et al., 2009). To robustly quantify IFN binding to cell-surface IFNAR, we probed binding of fluorescently labeled IFN $\alpha$ 2 wild type (IFN $\alpha$ 2-wt) to the cell surface in situ by total internal reflection fluorescence microscopy (TIRFM). For this purpose, we used site-specific labeling of IFN $\alpha$ 2-wt with DY647 via an N-terminal ybbR-tag (<sup>DY647</sup>IFN $\alpha$ 2-wt). Thus, a high fraction of labeled IFN $\alpha$ 2-wt (>90%) with a well-defined 1:1 labeling degree and uncompromised receptor binding was obtained (Waichman et al., 2010). Unspecific IFN binding to the cover slide surface was minimized by coating the glass slides with a protein-repelling poly(ethylene glycol) (PEG) polymer brush functionalized with an RGD peptide to promote cell adhesion (PLL-PEG-RGD). When HeLa cells cultured on PLL-PEG-RGD-coated cover slides were incubated with <sup>DY647</sup>IFN $\alpha$ 2-wt at saturating concentrations (2 nM), highly specific binding to the cell surface receptor could be observed on the single-molecule level (Fig. 1 b and [Video 1](#)). The majority ( $\sim 90\%$ ) of detected molecules were continuously diffusing, corroborating binding to cell surface receptors rather than to the cover slide surface (Fig. S1). For cells blocked with unlabeled IFN $\alpha$ 2-wt or for U5A cells, which do not express the high-affinity receptor subunit IFNAR2, negligible binding of <sup>DY647</sup>IFN $\alpha$ 2-wt was observed (Fig. 1 c and [Fig. S1](#)).

Under typical acquisition conditions optimized for unambiguous single-molecule detection, no significant bleaching was observed within a standard observation time of several seconds (Fig. 1 d). To confirm observation of individual ligand–receptor complexes rather than receptor clusters, imaging was performed at elevated excitation power, leading exclusively to single-step photobleaching events (Fig. 1, d–f; and [Video 2](#)). At a <sup>DY647</sup>IFN $\alpha$ 2-wt concentration sufficient to saturate all binding sites at the cell surface, a mean density of  $\sim 0.55$  molecules/ $\mu\text{m}^2$  was detected, corresponding to 500–1,000 binding sites per cell, which is in line with the estimated concentrations of IFNAR1 and IFNAR2 (François-Newton et al., 2011). While the number of detected molecules on the cell surface remained constant during typical experimental observation times at 25°C, a substantial decrease over time was observed at 37°C, which was ascribed to endocytosis of signaling complexes. To minimize the variability due to changes in cell surface concentrations, all further experiments were performed at 25°C.

Analysis of single-molecule trajectories revealed heterogeneous diffusion properties of <sup>DY647</sup>IFN $\alpha$ 2-wt bound to the cell surface receptor (Fig. 1 g) with a mean diffusion constant of  $0.094 \pm 0.011$   $\mu\text{m}^2/\text{s}$  ( $n = \sim 4,000$  trajectories), which is typical for a transmembrane receptor in the plasma membrane (Kusumi et al., 2012). The immobile fraction ( $\sim 10\%$ ) obtained by deconvolution of the step length histogram could be largely

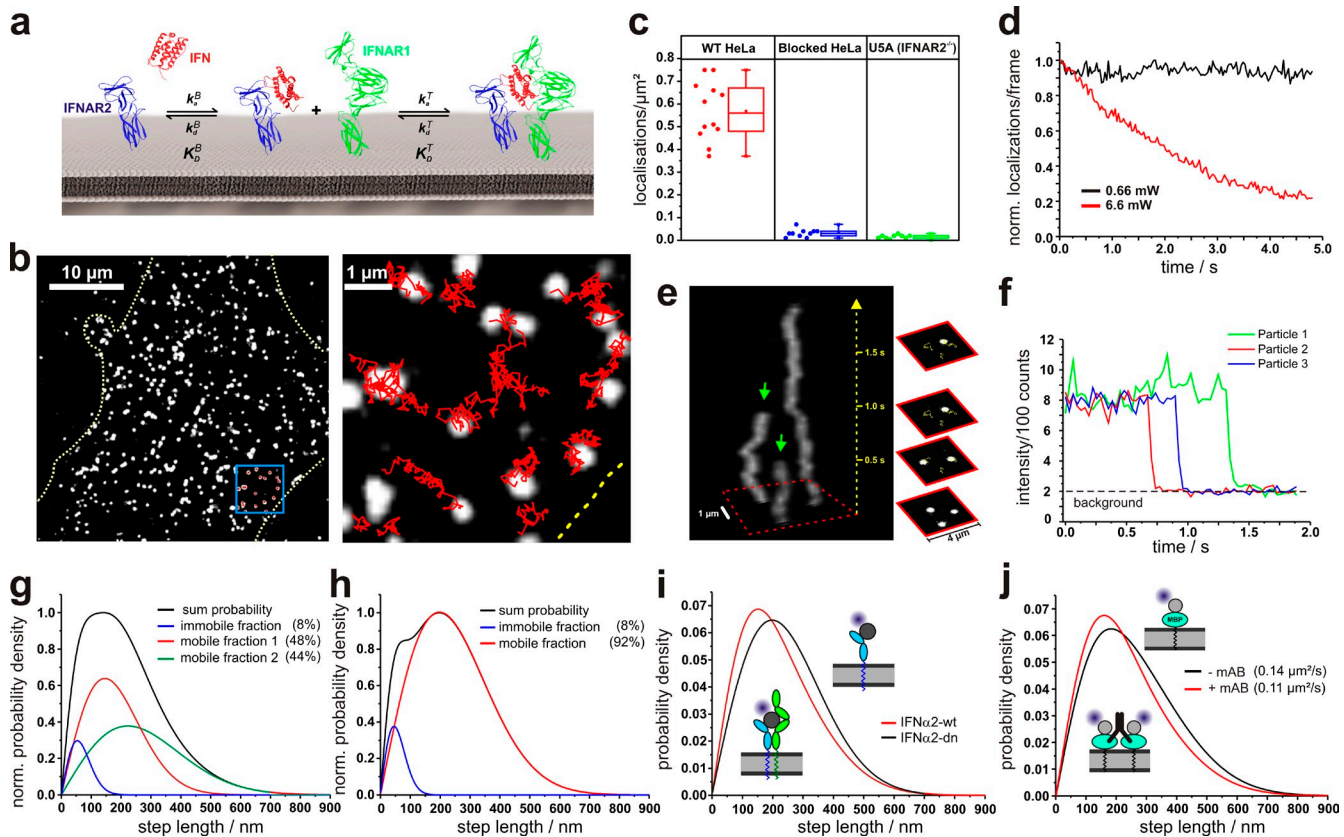


**Figure 1. Single-molecule localization and tracking of  $DY647$ IFN binding to endogenous cell surface IFNAR.** (a) Ligand-induced assembly of a dynamic ternary complex. The effective ligand binding affinity to the cell surface receptor depends on the dynamic equilibrium between the binary and ternary complex. (b) Live-cell IFN $\alpha$ 2 binding assay by single-molecule imaging on HeLa. (b, left) A fluorescence image showing individual  $DY647$ IFN $\alpha$ 2-wt bound to the cell surface receptor. (b, right) Trajectories of IFN $\alpha$ 2-wt molecules from the boxed region. The boundaries of the cell are indicated by a yellow dotted line. (c) Density of  $DY647$ IFN $\alpha$ 2-wt molecules localized on the surface of individual HeLa cells imaged in the presence of 2 nM  $DY647$ IFN $\alpha$ 2-wt. For comparison, the density of  $DY647$ IFN $\alpha$ 2-wt molecules on HeLa cells blocked with unlabeled IFN $\alpha$ 2-wt is shown in addition to IFNAR2-deficient U5A cells. Data distribution of the second and third quartile (box), median (line), mean (closed square), and whiskers (1.5 $\times$  interquartile range) is shown. (d) Normalized bleaching of  $DY647$ IFN $\alpha$ 2-wt (>150 particles at  $t = 0$ ) bound to endogenous receptors on HeLa at standard conditions and 10-fold increased laser power. Representative curves are shown for at least five experiments. (e) Single-step bleaching events of labeled IFNs depicted as a 3D kymograph. Bleaching events are indicated by green arrows. (f) Single-step bleaching events of three individually labeled IFNs (representative curves for >100 bleached particles). (g) Diffusion properties of cell-bound  $DY647$ IFN $\alpha$ 2-wt presented as the step length distribution for a time lapse of 160 ms (5 frames, black curve), which was obtained by fitting the step length histogram by considering three components corresponding to an immobile as well as a slow and a fast mobile fraction (Fig. S1). (h) Diffusion properties of cell-bound  $DY647$ IFN $\alpha$ 2-dn and fit according to a two-component model. (i) Comparison of the step-length histogram for  $DY647$ IFN $\alpha$ 2-wt and  $DY647$ IFN $\alpha$ 2-dn. The data shown in g–i are pooled from at least two independent experiments, each with >650 analyzed trajectories ( $\geq 15$  steps) per IFN mutant. (j) Changes in mobility of a model transmembrane protein dimerized by a monoclonal antibody. The data shown are pooled from eight independent experiments with >400 analyzed trajectories for each experiment ( $\geq 15$  steps).

ascribed to residual nonspecific binding of  $DY647$ IFN $\alpha$ 2-wt to the cover slide surface, but also included slow-diffusing molecules (Fig. S1). For more robust analysis of ligand binding and diffusion properties, immobile molecules were identified by a spatio-temporal clustering algorithm (DBSCAN; Sander et al., 1998; Roder et al., 2014) and removed before further analyses. Interestingly, an antagonistic IFN $\alpha$ 2-wt variant (IFN $\alpha$ 2-dn, for details see Table S1), which binds with 20-fold increased affinity to IFNAR2, but does not recruit IFNAR1 (Pan et al., 2008), showed significantly less heterogeneous diffusion properties (Fig. 1 h) and higher mobility compared with IFN $\alpha$ 2-wt (Fig. 1 i), with a mean diffusion constant of  $0.126 \pm 0.008 \mu$ m<sup>2</sup>/s ( $n = \sim 4,000$  trajectories;  $P < 0.001$ ). A comparable difference in mobility was observed for a model transmembrane protein (maltose-binding protein fused to a transmembrane helix) before and after dimerization by a monoclonal antibody (Fig. 1 j).

These findings are in line with ligand-induced receptor dimerization leading to reduced mobility of the receptor subunits.

### USP18 interferes with ligand binding to the cell surface receptor

For probing receptor dimerization and its regulation by USP18 via IFN binding assays, we used the IFN $\alpha$ 2 mutant M148A, which binds IFNAR2 with  $\sim 50$ -fold reduced affinity ( $K_d = \sim 150$  nM) compared with its wt form (Piehler et al., 2000; compare Table S1). At concentrations most suitable for in situ TIRFM binding assays (2 nM),  $DY647$ IFN $\alpha$ 2-M148A only binds significantly to the cell surface receptor when simultaneously interacting with both IFNAR1 and IFNAR2, and thus is an indirect marker for ternary complex formation. Compared with  $DY647$ IFN $\alpha$ 2-wt,  $\sim 60\%$  reduced binding of  $DY647$ IFN $\alpha$ 2-M148A ( $\sim 0.25$  molecules/ $\mu$ m<sup>2</sup>) to HeLa cells was observed (Fig. 2 a), which is in line with the

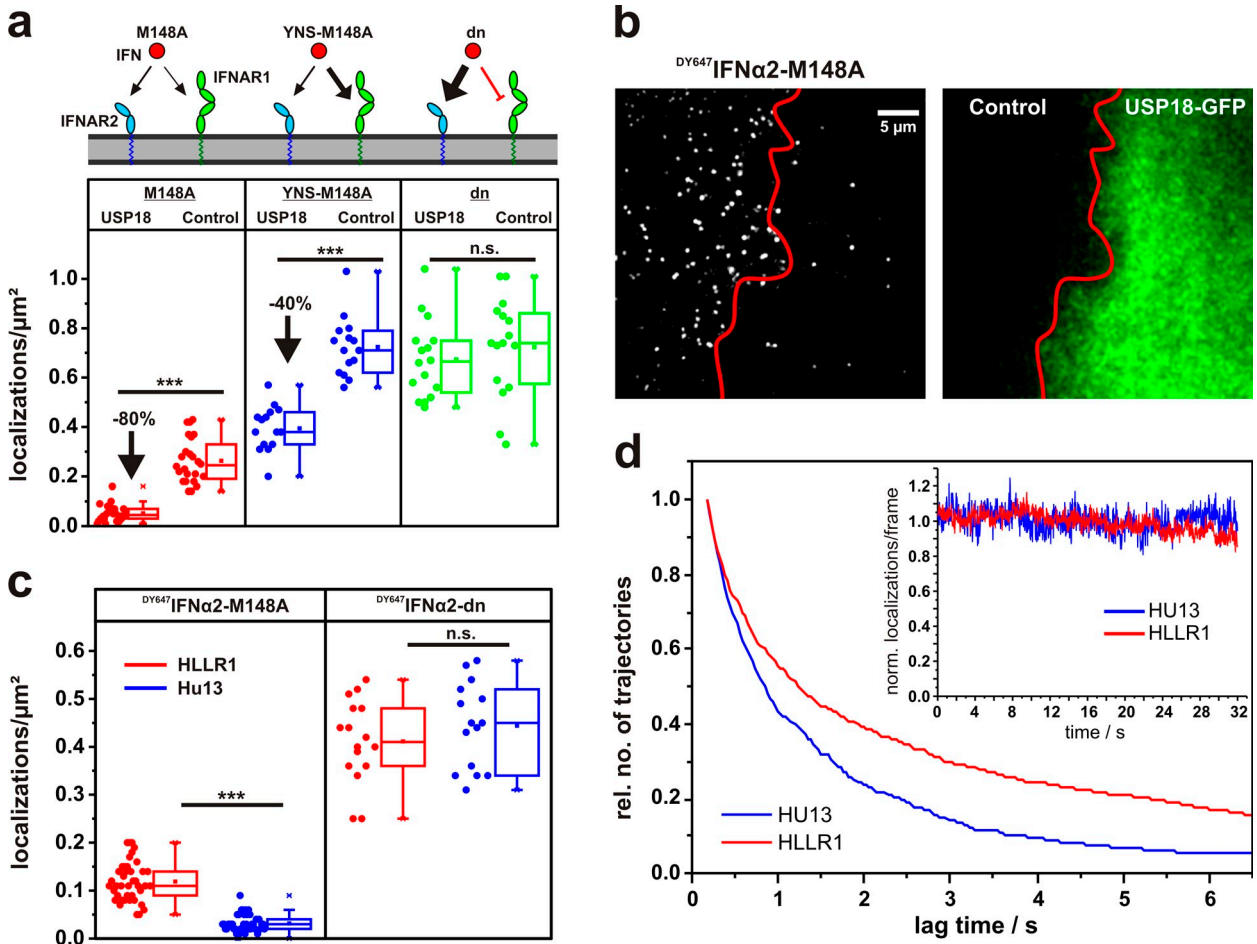


**Figure 2. The role of USP18 in receptor assembly probed by quantitative ligand-binding assays.** (a) Density of  $\text{DY}^{647}\text{IFN}\alpha 2\text{-M148A}$ ,  $\text{DY}^{647}\text{IFN}\alpha 2\text{-YNS-M148A}$ , and  $\text{DY}^{647}\text{IFN}\alpha 2\text{-dn}$  ( $\alpha 8\text{tail-R120E}$ ) on HeLa cells expressing USP18 and wt HeLa cells in comparison. (b) HeLa cells transiently transfected with EGFP-USP18 (green channel, right) after incubation of 2 nM  $\text{DY}^{647}\text{IFN}\alpha 2\text{-M148A}$ . For comparison, a nontransfected cell is shown in the same image. (c) Localization density in the presence of 2 nM  $\text{DY}^{647}\text{IFN}\alpha 2\text{-M148A}$  and  $\text{DY}^{647}\text{IFN}\alpha 2\text{-dn}$ , respectively, on cells stably transfected with USP18 (HU13) and to parental cells (HLLR1). \*\*\*,  $P > 0.001$ . (d) Life-time of  $\text{DY}^{647}\text{IFN}\alpha 2\text{-M148A}$  binding to HLLR1 and HU13 cells, respectively, as obtained by trajectory length analysis. Inset: bleaching control. The curves were obtained from  $>10$  independent experiments with  $>600$  analyzed trajectories ( $\geq 5$  steps) for HU13 and  $>1,000$  trajectories for HLLR1, respectively. Box plots indicate the data distribution of the second and third quartile (box), median (line), mean (closed squares), and whiskers (1.5 $\times$  interquartile range).

effective cell surface receptor binding affinity of 5–10 nM estimated for this mutant. Single-molecule diffusion analysis (Fig. S1) confirmed a substantially reduced mobility of  $\text{DY}^{647}\text{IFN}\alpha 2\text{-M148A}$  compared with  $\text{DY}^{647}\text{IFN}\alpha 2\text{-dn}$  ( $P < 0.001$ ), supporting efficient ternary complex formation by IFN $\alpha 2\text{-M148A}$ , which is in line with its capability to fully activate cellular responses (see the last paragraph of the Results section).

Upon expression of USP18, however, binding of  $\text{DY}^{647}\text{IFN}\alpha 2\text{-M148A}$  to the cell surface was substantially further reduced by  $\sim 80\%$  (Fig. 2, a and b; and Video 3). This effect was confirmed to be independent of the catalytic activity of USP18, as expression of the catalytically inactive mutant C61S induced a comparable decrease in  $\text{DY}^{647}\text{IFN}\alpha 2\text{-M148A}$  binding (Fig. S1). A similar phenotype was observed for HU13 cells, which stably express USP18 (Fig. 2 c and Fig. S1) and were previously established to study the negative feedback by USP18 (François-Newton et al., 2011). Trajectory length analysis of individual  $\text{DY}^{647}\text{IFN}\alpha 2\text{-M148A}$  bound to HU13 compared with parental HLLR1 cells moreover confirmed the increased rate of ligand

dissociation from the cell surface receptor in the presence of USP18 (Fig. 2 d and Video 4).

USP18 was found to interact with the cytoplasmic domain of IFNAR2 and thus potentially down-regulate cell surface expression or binding affinity of IFNAR2. We therefore quantified binding of  $\text{DY}^{647}\text{IFN}\alpha 2\text{-dn}$ , which does not interact with IFNAR1, in the presence of USP18. Notably, the binding levels observed for this mutant were not affected by expression of USP18 (Fig. 2, a and c). These observations suggested that rather than affecting the binding affinity to IFNAR2, USP18 affects the ability to recruit IFNAR1 to form a ternary complex. This conclusion was further corroborated by binding assays with  $\text{DY}^{647}\text{IFN}\alpha 2\text{-M148A-YNS}$ , in which the additional mutations (H57Y, E58N, Q61S) lead to a 50–100-fold increased affinity to IFNAR1 without substantially changing the affinity to IFNAR2 (Kalie et al., 2007; compare Table S1). For this mutant, increased binding was observed in both control cells and USP18-expressing cells (Fig. 2 a). The difference in binding levels was only 40%, suggesting that the enhanced IFNAR1 binding affinity can

partially compensate the effect of USP18. These results support a two-step assembly mechanism, in which USP18 regulates ternary complex formation by interfering with the recruitment of IFNAR1 on the cell surface.

### Ligand-induced receptor dimerization revealed at the single-molecule level

To directly probe receptor dimerization, IFNAR1 and IFNAR2 were N-terminally fused to the HaloTag and the SNAPf-tag, respectively, for posttranslational labeling with photostable fluorescent dyes, and U5A cells stably expressing HaloTag-IFNAR1 and SNAPf-IFNAR2 at near-physiological level were generated (Fig. S2). The functional properties of these cells with respect to JAK and signal transducer and activator of transcription (STAT) phosphorylation (Fig. 3 a) and STAT1 nuclear translocation (Fig. 3 b) matched those of wt cell lines such as HeLa. Moreover, USP18 expression and its differential negative feedback to IFN $\alpha$ 2 and IFN $\beta$  signaling with respect to STAT phosphorylation was observed (Fig. 3 a), making these cells a viable system for our mechanistic studies. Upon dual-color single-molecule imaging by TIRFM after labeling with HaloTag tetramethyl rhodamine (TMR) ligand and SNAP-Surface 647, respectively, individual IFNAR1 and IFNAR2 could be clearly discerned (Video 5). A typical density of 1–3 molecules/ $\mu\text{m}^2$  was observed, i.e., 2–5-fold higher compared with the endogenous receptor level in HeLa cells estimated by ligand-binding experiments described in the “Single-molecule IFN binding and diffusion” section. Highly specific labeling of IFNAR1 and IFNAR2 was confirmed, as  $<0.04$  molecules/ $\mu\text{m}^2$  could be detected for nontransfected U5A labeled under the same conditions (Fig. S2).

Receptor dimerization was explored by single-molecule tracking and colocomotion analysis (Dunne et al., 2009) as schematically depicted in Fig. S2: individual IFNAR1 and IFNAR2 molecules in each frame were localized beyond the diffraction limit with an average precision of  $\sim 20$  nm, and trajectories were obtained by tracking individual molecules over multiple frames. For colocomotion analysis, tracking was performed exclusively with IFNAR1 and IFNAR2 molecules colocalized in each frame within 100 nm for  $\geq 10$  consecutive steps ( $\sim 300$  ms). Thus, stochastic colocalization was effectively eliminated (Ruprecht et al., 2010a), as confirmed by a negative control experiment with noninteracting molecules (Fig. S3 and Video 6). While in the absence of IFN no colocomotion of IFNAR1 and IFNAR2 was detectable, strong colocomotion ( $\sim 15\%$  with respect to IFNAR2) was observed upon addition of IFN $\alpha$ 2-wt at saturating concentrations (Fig. 3, c and e; and Video 7). The formation of individual 1:1 complexes was confirmed by single-molecule bleaching experiments (Video 8). More detailed trajectory analysis revealed the dynamic formation of ternary complexes, as both association and dissociation events of individual complexes could be discerned (Fig. 3 d and Video 9). To correctly quantify the number of dimerized receptors from the fraction of colocomotion events, we used a positive control with both the HaloTag and the SNAPf-tag fused to IFNAR2 (Fig. S3). Under these conditions,  $\sim 20\%$  of the trajectories showed colocomotion (Fig. 3 e), which was taken as a reference for 100% complex formation. Thus, 70–80% of

IFNAR2 was recruited into ternary complexes upon stimulation with IFN $\alpha$ 2-wt.

To test the possibility of very transient receptor dimerization, which would not be picked up by the colocomotion assay, we analyzed spatial co-organization of IFNAR1 and IFNAR2 by particle image cross-correlation spectroscopy (Semrau et al., 2011; Fig. S3). These studies clearly excluded receptor predimerization or co-organization of IFNAR1 and IFNAR2 in the absence of ligand and confirmed efficient dimerization by IFN $\alpha$ 2-wt (Fig. S3). Ligand-induced ternary complex assembly could also be detected by analyzing the diffusion properties as shown in Fig. 3 f. For dimerized IFNAR1 and IFNAR2, significantly reduced mobility was observed compared with the subunits in the absence of ligand (Fig. 3 f). These findings corroborate that the reduced mobility observed for <sup>DY647</sup>IFN $\alpha$ 2-wt compared with <sup>DY647</sup>IFN $\alpha$ 2-dn (compare Fig. 1 i) was caused by receptor dimerization. By decomposing the distribution observed for the total population of IFNAR1 and IFNAR2 in the presence of IFN $\alpha$ 2-wt, a fraction of  $\sim 70\%$  IFNAR2-bound IFN $\alpha$ 2-wt in complex with IFNAR1 was estimated. These results support the two-step assembly model depicted in Fig. 1 a, and highlight the relevance of equilibrium between binary (IFN/IFNAR2) and ternary complexes (IFN/IFNAR2/IFNAR1) at physiological receptor levels.

### IFNAR1 binding affinity of IFN $\alpha$ 2-wt is optimized for efficient ternary complex formation

Based on the colocomotion assay, we systematically explored IFNAR dimerization by different IFN subtypes and mutants with altered binding affinities toward IFNAR1. IFN $\beta$  and IFN $\alpha$ 2-YNS, which both bind IFNAR1 50–100-fold stronger than IFN $\alpha$ 2-wt (compare with Table S1), yielded dimerization levels slightly higher than IFN $\alpha$ 2 (Fig. 4 a). By comparison with the maximum level observed in the positive control,  $\sim 85\%$  dimerization can be estimated for IFN $\beta$  and IFN $\alpha$ 2-YNS, compared with  $\sim 70\%$  dimerization achieved by IFN $\alpha$ 2-wt. Importantly, dimerization was independent of signal activation, since a similar level of colocomotion was observed for IFN $\alpha$ 2-wt in the presence of a JAK inhibitor. These results suggest that the receptor concentrations substantially exceed the two-dimensional binding equilibrium constant  $K_D^T$  (compare with Fig. 1 a) even in the case of IFN $\alpha$ 2-wt. However, upon introducing mutations into IFN $\alpha$ 2, which reduce the binding affinity toward IFNAR1 (Roisman et al., 2005; Pan et al., 2008), significantly decreased receptor dimerization could be observed (Fig. 4 a). By using quantitative receptor dimerization experiments on solid-supported membranes in vitro (Gavutis et al., 2005) to determine the relative binding affinities of these mutants (Fig. S4), we established a quantitative affinity–dimerization relationship, as depicted in Fig. 4 b. The sigmoidal shape observed for this correlation is in line with the law of mass action governing the equilibrium between binary and ternary complexes, as depicted in Fig. 1 a. The maximum amplitude of  $<100\%$  colocomotion observed in this plot could be at least partially explained by endogenous IFNAR1, which further reduces the effective degree of labeling. Based on this affinity–dimerization relationship, we estimated a two-dimensional

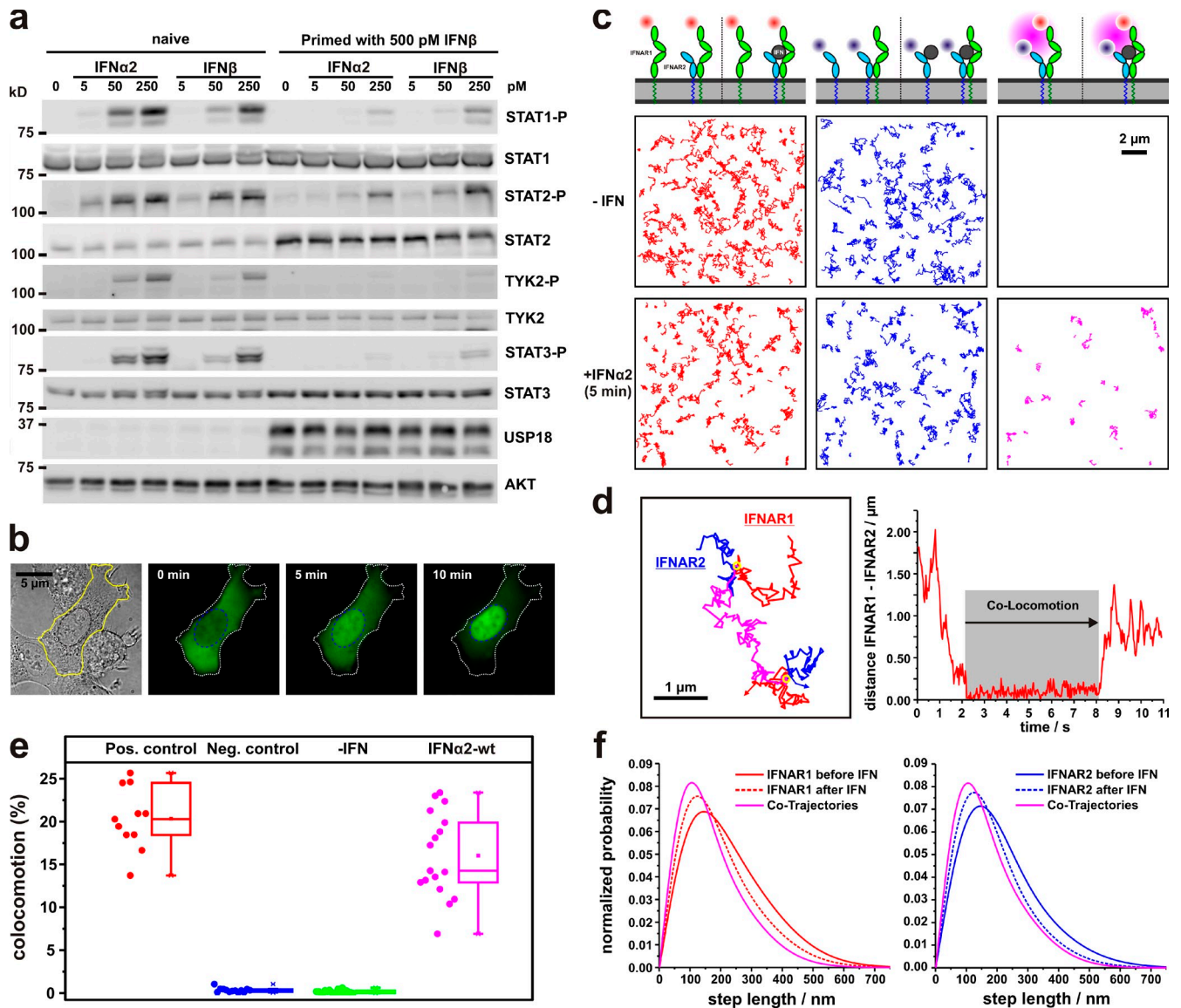


**Figure 3. Receptor dimerization probed by single-molecule colocomotion analysis.** (a and b) Functional properties of U5A cells, which were stably complemented with tagged IFNAR1 and IFNAR2 (U5A<sup>IFNAR1/IFNAR2</sup>) for posttranslational labeling and single-molecule imaging. (a) Western blot analysis of STAT phosphorylation, USP18 expression, and differential desensitization to IFN $\alpha$ 2 and IFN $\beta$ . (b) IFN-induced translocation of STAT1-EGFP into the nucleus. (c) IFN-induced receptor dimerization revealed by single-molecule colocomotion experiments. Trajectories (80 frames,  $\sim$ 2.5 s) of individual TMR-labeled IFNAR1 (red), DY647-labeled IFNAR2 (blue), and co-trajectories (magenta) in the absence and presence of 50 nM IFN $\alpha$ 2 are shown. The diagram above indicates the possible different species detected in each channel before (left) and after (right) addition of the ligand, taking unlabeled IFNAR1 and IFNAR2 into account. (d) Formation and dissociation of an individual IFNAR1-IFNAR2 dimer in the presence of IFN $\alpha$ 2 as observed by an overlay of the individual trajectories (left) and by a distance analysis (right). Shown is a representative curve from >25 curves analyzed. (e) Relative number of colocomotion trajectories for dual-labeled IFNAR2 (positive control) and noninteracting proteins (negative control), as well as IFNAR1 and IFNAR2, in the absence and presence of IFN $\alpha$ 2. The box plot indicates the data distribution of the second and third quartile (box), median (line), mean (filled square), and whiskers (1.5 $\times$  interquartile range). (f) Diffusion properties represented as step-length distribution of IFNAR1 (left; from >800 trajectories) and IFNAR2 (right; from >500 trajectories) in the absence and presence of IFN $\alpha$ 2. For comparison, the step-length distribution of colocomotion trajectories (+IFN $\alpha$ 2) is shown (from  $\sim$ 100 trajectories).

binding affinity  $\kappa_D^I$  of 0.29 molecules/ $\mu$ m<sup>2</sup> for the interaction of IFNAR1 with IFN $\alpha$ 2-wt bound to IFNAR2 (Table 1). The  $\kappa_D^I$  of IFN $\beta$  is too low to be directly quantified at these receptor surface concentrations, but can be estimated to be 0.005 molecules/ $\mu$ m<sup>2</sup> based on the relative IFNAR1 binding affinity. Thus, in contrast to IFN $\beta$ , the binding affinity of IFN $\alpha$ 2-wt toward IFNAR1 is at the edge in order to still allow efficient ternary complex formation at physiological receptor expression levels.

### USP18 modulates receptor dimerization efficiency

Based on this quantitative dimerization assay, we next tested the effect of USP18 on the dimerization efficiency. To obtain reproducible and physiologically relevant levels of USP18 in U5A cells stably transfected with HaloTag-IFNAR1 and SNAPf-IFNAR2, we primed cells with IFN (François-Newton et al., 2011), thus inducing the same phenotype as ectopic USP18 expression (Fig. S5). To ensure efficient washout, we used IFN $\alpha$ 2-M148A

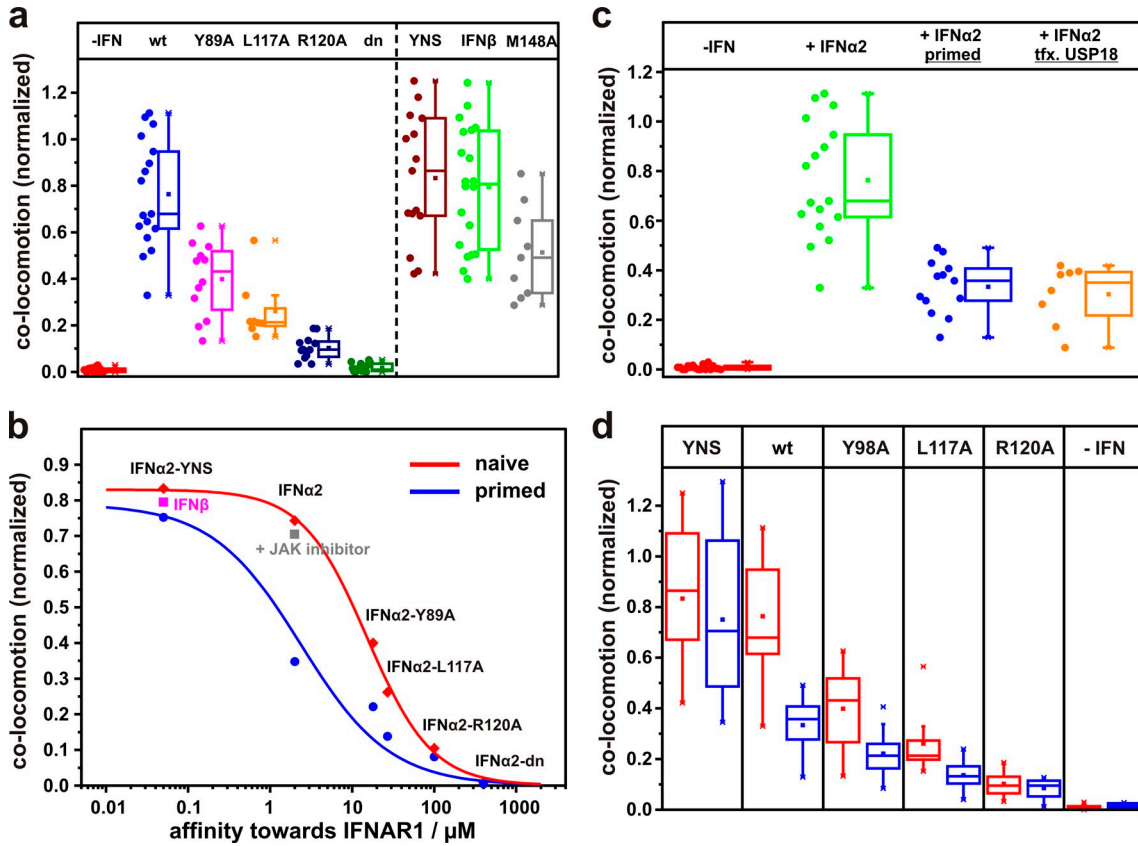


Figure 4. **IFNAR dimerization observed for different IFN subtypes and mutants.** (a) Relative number of colocomotion trajectories detected in the absence of ligand, in the presence of wt IFN $\alpha$ 2, and in several IFN $\alpha$ 2 mutants with increased and decreased binding affinities toward IFNAR1 and IFN $\beta$  (each 50 nM) and IFN $\alpha$ 2-M148A (200 nM). The broken line separates different types of mutants. (b) Affinity–dimerization relationship and plot of the law of mass action for naive and primed cells (data points are mean values taken from d). Dimerization for IFN $\beta$  is included as well as for IFN $\alpha$ 2-wt under JAK inhibition. (c) Receptor dimerization in U5A<sup>IFNAR1/IFNAR2</sup> cells in the absence and presence of 50 nM IFN $\alpha$ 2, and after priming and ectopic expression of (EGFP)-USP18. (d) Comparison of colocomotion events for 50 nM IFN $\alpha$ 2-wt and mutants observed with naive (red) and primed cells (blue). Box plots indicate the data distribution of the second and third quartile (box), median (line), mean (closed squares), and whiskers (1.5 $\times$  interquartile range).

for priming, which is as able to desensitize cells as IFN $\alpha$ 2-wt (Fig. S5). Colocomotion assays in primed cells revealed a substantial decrease in receptor dimerization by IFN $\alpha$ 2-wt and all mutants with reduced binding affinity toward IFNAR1 (Fig. 4, c and d). This was also true for cells ectopically expressing USP18 (Fig. 4 c). These observations clearly established that negative feedback via USP18 affects receptor dimerization. In contrast, only minor changes in receptor dimerization by IFN $\alpha$ 2-YNS were observed in IFN-primed cells (Fig. 4 d). The quantitative affinity–dimerization relationship obtained in the presence of USP18 is in line with a general shift in the two-dimensional binding affinity  $K_D^I$  (Fig. 4 b). For the interaction of IFNAR1 with IFN $\alpha$ 2-wt bound to IFNAR2 in the presence of USP18, a  $K_D^I$  of 4.3 molecules/ $\mu\text{m}^2$  was estimated (Table 1), i.e., an  $\sim$ 15-fold increase compared with the interaction in naive cells. These observations clearly established that USP18 acts by attenuating IFNAR1 recruitment into the ternary complex by reducing the 2D affinity.

#### Associated JAKs stabilize the ternary complex

USP18 has been shown to bind to the cytosolic domain of IFNAR2 and desensitize cells with respect to STAT phosphorylation, independently of its catalytic activity. We therefore hypothesized

that USP18 weakens cytosolic interactions between the receptor subunits, which stabilize the ternary complex. Indeed, reduced receptor dimerization by IFN $\alpha$ 2-wt, but not IFN $\alpha$ 2-YNS, was observed on cells expressing IFNAR2  $\Delta$ 265 that lack the cytosolic domain (Fig. 5 a and Table 1). Moreover, dimerization efficiencies were similar to those measured in the presence of USP18. Because USP18 has been suggested to interfere with Jak1 binding to IFNAR2 (Malakhova et al., 2006), we explored in more detail the role of Jak1 for receptor dimerization. Strikingly, similar dimerization levels were observed for full-length

Table 1. **IFNAR1/IFNAR2 heterodimer fraction  $\alpha$  observed for IFN $\alpha$ 2-wt and  $K_D^I$  obtained from the law of mass action**

Experimental conditions	$\alpha$	$K_D^I$ <sup>a</sup>
IFNAR2-fl	0.89	$\mu\text{m}^{-2}$ 0.29
IFNAR2-fl (primed)	0.41	4.3
IFNAR2 ( $-\Delta$ 346)	0.84	0.46
IFNAR2 ( $-\Delta$ 265)	0.36	5.4

<sup>a</sup>Calculated from mean experimental receptor concentrations corrected for the degree of labeling (IFNAR1, 3.5  $\mu\text{m}^{-2}$ ; IFNAR2, 1.3  $\mu\text{m}^{-2}$ ). Experimental error:  $\pm$ 50%.

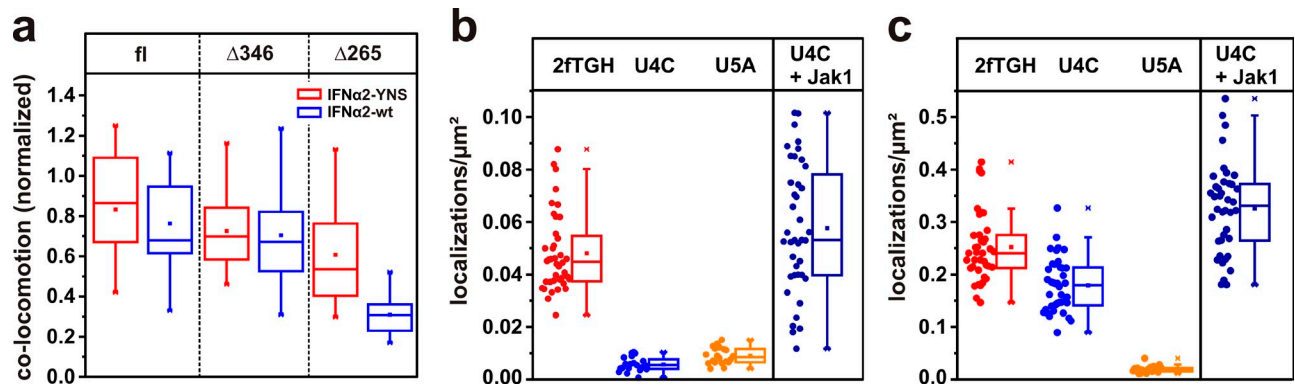


Figure 5. **The role of Jak1 in stabilizing the ternary complex.** (a) Receptor dimerization by IFN $\alpha$ 2 (blue) and IFN $\alpha$ 2-YNS (red) for full-length (fl) IFNAR2, IFNAR2 truncated after the Jak1 binding site ( $\Delta$ 346), and after the transmembrane domain ( $\Delta$ 265). (b and c) Binding of 2 nM <sup>DY647</sup>IFN $\alpha$ 2-M148A (b) and <sup>DY647</sup>IFN $\alpha$ 2-dn (c) to cell lines deficient in Jak1 (U4C) and IFNAR2 (U5A). For comparison, binding to the parental cell line (2fTGH) and to U4C complemented with Jak1 is shown. Box plots indicate the data distribution of the second and third quartile (box), median (line), mean (closed squares), and whiskers (1.5 $\times$  interquartile range).

IFNAR2 and for IFNAR2 ( $-\Delta$ 346) that is truncated after the Jak1 binding site (Fig. 5 a), which supports the finding that ternary complex stabilization may be mediated via the JAKs. From the  $\sim$ 18-fold difference in the  $K_D^T$  in the absence and in the presence of the cytosolic domain of IFNAR2, an energetic contribution of  $\sim$ 7.1 kJ/mol can be estimated from the interactions between the receptor subunits in the cytosol.

We further investigated the role of Jak1 for receptor dimerization using <sup>DY647</sup>IFN $\alpha$ 2-M148A binding assays in the Jak1-deficient cell line U4C. While binding of IFN $\alpha$ 2-M148A was comparable on parental 2fTGH, HeLa, and HLLR1 cells, binding on U4C cells was found to be negligible (Fig. 5 b) but was recovered upon complementation with Jak1. Binding experiments with IFN $\alpha$ 2-dn confirmed essentially unaltered expression of IFNAR2 in U4C cells (Fig. 5 c). Overall, these observations strongly suggest that Jak1 association to IFNAR2 further stabilizes the ternary signaling complex and that USP18 interferes with this interaction, e.g., by outcompeting Jak1.

#### USP18 phenotype can be mimicked by IFNs with reduced IFNAR1 binding affinity

An important consequence of reduced receptor dimerization efficiency upon expression of USP18 would be the loss of functional signaling complexes on the membrane, which cannot be compensated by increasing the ligand concentration in solution. Fewer signaling active complexes would in turn affect the maximal STAT phosphorylation level. We therefore explored the role of receptor dimerization for STAT phosphorylation by performing dose–response assays for different IFN $\alpha$ 2 variants in the absence (HLLR1 cells) and presence (HU13 cells) of USP18. As expected, dose–response curves revealed a substantial reduction in the maximum level of STAT phosphorylation (pSTAT1 and pSTAT2) upon ectopic expression of USP18 (Fig. 6). Indeed, the maximum amplitudes of pSTAT1 and pSTAT2 were reduced by  $\sim$ 75% and  $\sim$ 50%, respectively, which is in line with the reduced maximum number of ternary complexes formed in the presence of USP18 (compare with Table 1). For IFN $\alpha$ 2-R120A, a mutant with  $\sim$ 60-fold reduced IFNAR1 binding affinity, a similar reduction in the maximum

binding amplitude was already observed in the absence of USP18. In contrast, for IFN $\alpha$ 2-M148A, with its  $\sim$ 50-fold reduced binding affinity toward IFNAR2, the same maximum level of STAT phosphorylation as for IFN $\alpha$ 2-wt was still obtained, though at higher ligand concentrations. Thus, reduction of IFN affinity toward IFNAR1 mimics the phenotype observed for USP18, corroborating the fact that USP18 regulates IFN signaling on the level of IFNAR1 recruitment.

## Discussion

In this study, we have attempted to uncover the mechanistic basis of IFN receptor plasticity regulated by the negative feedback inhibitor USP18, which was previously shown to be a key determinant for differential activity of IFN $\alpha$ 2 and IFN $\beta$ . Because USP18 was shown to affect ligand binding, we focused our studies on the assembly of the IFN signaling complex. During the past decade, the mechanism of cytokine receptor assembly has been a matter of controversy because for several homodimeric class I cytokine receptors, ligand-independent predimerization of the receptor subunits has been demonstrated (Remy et al., 1999; Constantinescu et al., 2001; Brown et al., 2005; Yang et al., 2007). A similar mechanism was proposed for heterodimeric class I (Damjanovich et al., 1997; Tenhumberg et al., 2006; Zaks-Zilberman et al., 2008) and class II receptors (Krause et al., 2002, 2006a,b), including the IFN receptor (Krause et al., 2013). Here, we have unambiguously shown that IFNAR1 and IFNAR2 are not preassembled in the plasma membrane of living cells, but are efficiently dimerized upon IFN binding. Revealing this assembly mechanism was made possible by exploiting and optimizing single-molecule fluorescence imaging techniques, which allowed studying receptor assembly at a physiological expression level, an absolutely critical prerequisite, as the rate and affinity constants of IFN–receptor interactions are fine-tuned for receptor concentrations corresponding to only a few hundred copies per cell. Quantitative ligand-binding studies with site-specifically labeled IFNs revealed random and nonclustered distribution of signaling complexes at the cell surface at densities of  $<1/\mu\text{m}^2$ , which is ideally suitable for single-molecule imaging techniques. While

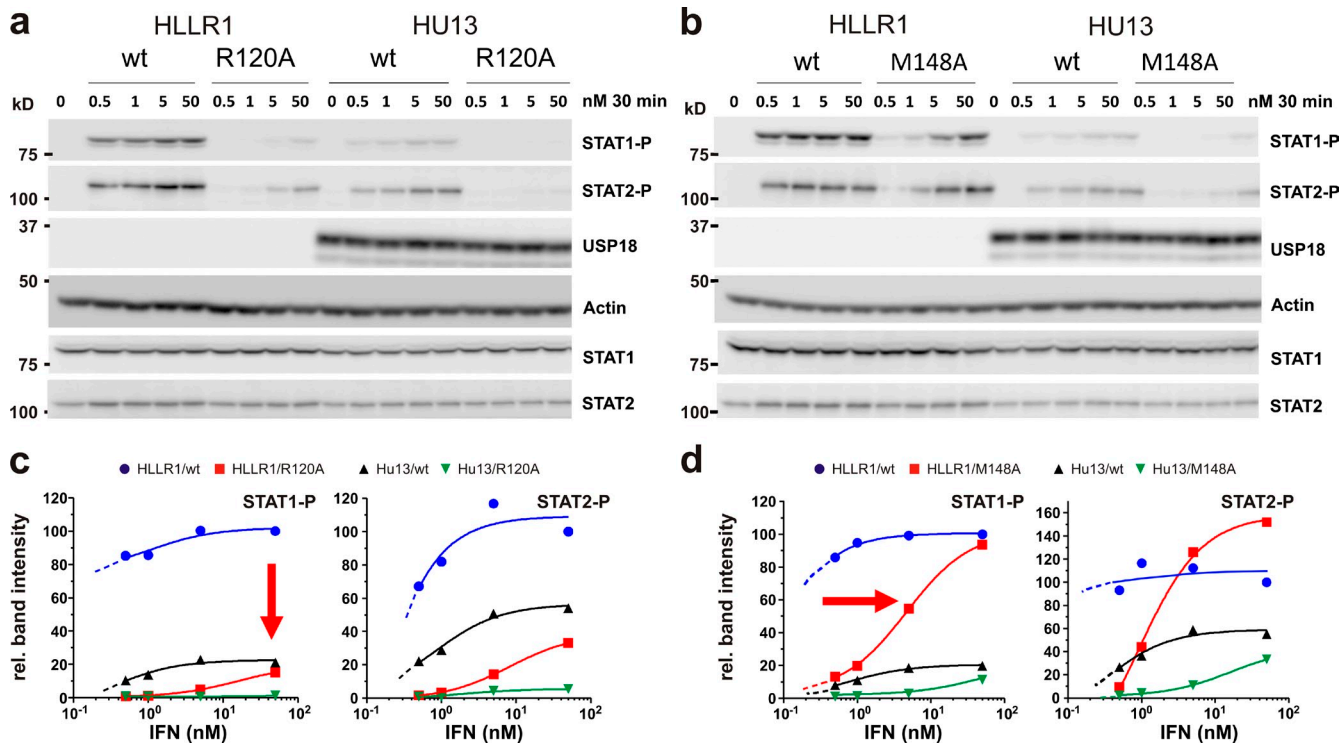


Figure 6. **Functional consequences of USP18-mediated interference with ternary complex assembly.** (a and b) Western blot analysis of STAT1 and STAT2 phosphorylation in parental HLLR1 cells versus cells stably expressing USP18 (HU13) stimulated with IFN $\alpha$ 2-wt, -R120A, or -M148A. (c and d) Dose-response curve for pSTAT normalized to total STAT calculated from the band intensities in the Western blot (representative data from three independent experiments). Values were normalized to those obtained at the highest dose of IFN wt, which was taken as 100%. The broken lines represent the curve extrapolations for lower IFN doses expected from independent experiments.

diffusion analysis for mutants with different receptor binding characteristics supported the model of IFN-induced dimerization of the endogenous receptor, dual-color single-molecule imaging was applied to identify the mechanism of receptor assembly. Based on posttranslational labeling of ectopically expressed IFNAR1 and IFNAR2 via fusion proteins with bright and photostable organic fluorescence dyes, we succeeded in monitoring IFN-stimulated dimerization and the formation of ternary complexes, which dynamically form and dissociate in the plasma membrane.

Importantly, preassembly of the receptor subunits could be excluded at these receptor concentrations. In contrast to traditional fluorescent proteins, the HaloTag and the SNAPf-tag are strictly monomeric and thus do not promote dimerization. Previous studies claiming IFNAR predimerization (Krause et al., 2013) may have been biased by the much higher ( $\sim 100$ -fold) receptor expression levels required for conventional fluorescence imaging techniques as well as by the interaction between GFP derivatives used for FRET (Shimozono and Miyawaki, 2008). We could not observe any spatial co-organization of IFNAR1 and IFNAR2 in the absence of IFN either, as has been previously suggested for several cytokine receptors (Vámosi et al., 2004; de Bakker et al., 2008; Jenei et al., 2009). This is in line with the observation that IFN signaling is independent of membrane microdomains (Marchetti et al., 2006). Yet, we revealed stabilization of the ternary complex via the associated JAKs, which suggests a productive interaction between Jak1 and Tyk2 in the signaling complex. Such productive contacts have been experimentally demonstrated for the epidermal growth factor

receptor tyrosine kinase domains (Zhang et al., 2006) and have been recently proposed for Jak2 in the growth hormone receptor complex (Brooks et al., 2014). Interestingly, previous studies suggesting receptor predimerization identified a critical role of JAKs in this process (Krause et al., 2013). Yet, the  $<3 k_B T$  binding energy we found for this interaction is clearly not sufficient for predimerization at physiological receptor expression levels.

Quantitative receptor dimerization studies at physiological expression levels allowed us to assess the role of IFNAR1 binding affinity in receptor assembly. Interestingly, at physiological receptor expression levels, the relatively low IFNAR1 binding affinity of IFN $\alpha$ 2 allows  $\sim 50\%$  of IFNAR2-bound IFN $\alpha$ 2 to form ternary complexes with IFNAR1 (Table S2). Notably, recruitment of the  $\gamma_c$  chain by IL-4 bound to its high-affinity receptor subunit has been indirectly shown to yield  $\sim 90\%$  dimerization (Whitty et al., 1998), which is in line with the  $\sim 10$ -fold lower  $K_d$  of the IL-4/ $\gamma_c$  compared with the IFN $\alpha$ 2-IFNAR1 interaction. However, this gives rise to the question of whether the IFNAR1 binding affinity of IFN $\alpha$ 2 (and other IFN $\alpha$  subtypes) is optimized to be most sensitive to changes in dimerization efficiency caused by the negative feedback regulator USP18. Here we found that USP18 shifts the equilibrium from the ternary toward the binary complex, probably by interfering with the cytosolic interactions between the receptor subunits, which are related to the associated JAKs. Intriguingly, the 2D affinity for IFN $\alpha$ 2-wt observed for feedback inhibition by USP18 in primed cells ( $K_D^T = 4.3 \mu\text{m}^{-2}$ ) reaches very similar levels as in the absence of cytosolic interactions in the case of IFNAR2- $\Delta 265$  ( $K_D^T = 5.4 \mu\text{m}^{-2}$ ). This effect

is independent of the catalytic activity of USP18, which suggests that USP18 binding to IFNAR2 (Malakhova et al., 2006; Löchte et al., 2014) directly interferes with complex stabilization via the intracellular domains. Interestingly, USP18 has been proposed to compete with Jak1 association to IFNAR2 (Malakhova et al., 2006), which again points toward a critical role of JAKs in stabilizing the ternary complex.

In the presence of USP18, IFN $\alpha$  subtypes lose their ability to efficiently recruit IFNAR1 into the signaling complexes. As the cell surface equilibrium is shifted toward the binary complex, the effective binding affinity of IFN $\alpha$ 2 to the cell surface receptor is reduced due to the increased dissociation kinetics as described in the “Single-molecule IFN binding and diffusion” section, which is in line with the shifted dose–response curve in the presence of USP18. In contrast, the substantially higher IFNAR1 binding affinity of IFN $\beta$  still ensures efficient receptor dimerization. This mechanism readily explains how IFN $\beta$  can maintain signaling much longer than IFN $\alpha$ 2 (François-Newton et al., 2011; François-Newton et al., 2012), which can account for its specific activities with respect to cell proliferation and differentiation (Uzé et al., 2007). As the concentration of USP18 is constantly changing after IFN stimulation, fine-tuning of cellular responsiveness against IFN subtypes is achieved. Two important implications of this desensitization mechanism are that (1) it can only partially be compensated by IFN concentrations, as the maximum number of complexes is limited by the IFNAR1 binding affinity; and (2) it can be eluded by an increased receptor cell surface expression. Indeed, differential signaling by IFN $\alpha$ 2 and IFN $\beta$  has been demonstrated to require relatively low receptor expression levels (Moraga et al., 2009; Levin et al., 2011). Likewise, differential signaling has been increased by further decreasing the IFNAR1 binding affinity of IFN $\alpha$ 2, thus yielding an IFN with antiviral, but not antiproliferative, activity (Levin et al., 2014), which can be explained by more efficient signal abrogation by USP18. For other IFN $\alpha$  subtypes, a very similar effect as for IFN $\alpha$ 2 can be expected, as they all bind IFNAR1 with similar affinity (Lavoie et al., 2011). Notably, the IFNAR binding properties of IFN $\alpha$ 1 are closely mimicked by IFN $\alpha$ 2-M148A, which we found here to be highly affected by USP18.

Functional plasticity has emerged as a frequent feature in cytokine signaling, which has been linked to differences in ligand binding affinities and interaction rate constants in several cases, e.g., for the IL-2/IL-15 receptor (Ring et al., 2012), the IL-10 receptor (Yoon et al., 2005, 2012), and the IL-4 receptor (LaPorte et al., 2008; Junttila et al., 2012). The novel mechanistic concept of differential IFN $\alpha$ / $\beta$  signaling being regulated at the level of receptor assembly may thus provide a general paradigm for cytokine receptor plasticity. Comprehensive understanding of functional receptor plasticity therefore will require characterizing the temporal evolution of signaling and its regulation by spatial and temporal feedback mechanisms in much more detail.

## Materials and methods

### Plasmid constructs

Ectopic expression of proteins in human cell lines was done under the control of the cytomegalovirus (CMV) promoter using the vector backbones of pSems-26m (Covalys Biosciences) and pDisplay (Invitrogen). Plasmids for

expression of IFNAR1 fused to an N-terminal HaloTag (pSems-neo HaloTag-IFNAR1) and IFNAR2c fused to an N-terminal SNAPf-tag (pSems-puro SNAPf-IFNAR2c) were generated as follows: the genes of full-length IFNAR1 and IFNAR2, respectively, without the N-terminal signal sequences were inserted into pDisplay (Invitrogen) via BglIII and PstI restriction sites. Subsequently, genes coding for the HaloTag and SNAPf-tag, respectively, were inserted via the BglIII site. The constructs including the signal sequence of the pDisplay vector (Ig $\kappa$ ) were transferred by restriction with EcoRI and NotI into modified versions of pSems-26m (Covalys Biosciences) linking the ORF to a neomycin or puromycin resistance cassette, respectively, via an IRES site. Truncations of the SNAPf-IFNAR2c (after residue no. 265, IFNAR2- $\Delta$ 265, and after residue no. 346, IFNAR2- $\Delta$ 346) were cloned by PCR and inserted accordingly. USP18 (a gift from Sylvie Urbé, University of Liverpool, Liverpool, England, UK) N-terminally fused to mEGFP was inserted into pSems via EcoRI and NotI. pSems-puro STAT1-mEGFP was generated by insertion of STAT1 via NotI and EcoRV. A positive control for single-molecule colocalization was cloned by insertion of the fusion construct HaloTag-SNAPf-IFNAR2c into pDisplay by EcoRI and PstI. For negative controls, we used fusion constructs of either HaloTag or SNAPf-tag with maltose-binding protein (MBP) linked to an artificial transmembrane domain K(ALA)<sub>7</sub>KSSR. SNAPf-MBP-TMD and HaloTag-MBP-TMD were inserted into pSems-neo and pSems-puro via EcoRV and NotI.

### Protein expression and purification

IFN $\alpha$ 2 and mutants fused to an N-terminal ybBR-tag (Yin et al., 2005; IFN $\alpha$ 2, IFN $\alpha$ 2-YNS, IFN $\alpha$ 2-M148A, IFN $\alpha$ 2-YNS-M148A, and IFN $\alpha$ 2- $\alpha$ 8tail-R120E, “dn”) for site-specific posttranslational labeling were cloned by insertion of an oligonucleotide linker coding for the ybBR peptide (DSLEFIASKLA) into the NdeI restriction site upstream of the corresponding genes in the plasmid pT7T3-U18cis (Piehler and Schreiber, 1999a). Proteins were expressed in *Escherichia coli* (TG1 strain) at 37°C. After solubilization of inclusion bodies and refolding by dilution with 0.8 M arginine (Kalie et al., 2007), the proteins were purified by anion exchange chromatography (HiTrap Q; GE Healthcare) with a NaCl gradient at pH 8.0, as described previously for wt IFN $\alpha$ 2 (Piehler et al., 2000). The proteins labeled with DY 647 (Dyomics) were conjugated to Coenzyme A via enzymatic phosphopantetheinyl-transfer (PPT) using the PPTase Sfp according to published protocols (Yin et al., 2005). After the labeling reaction, IFNs were purified by size exclusion chromatography (Superdex 75; GE Healthcare) in 20 mM Hepes, pH 7.5, and 150 mM NaCl (Hepes-buffered saline [HBS]) as described previously (Waichman et al., 2010). A >90% degree of labeling was obtained for all IFN $\alpha$ 2 proteins, as determined by UV/Vis spectroscopy. IFN $\beta$  was obtained from D. Baker (Biogen Idec Inc., Cambridge, MA). The extracellular domain of IFNAR1 with a C-terminal decahistidine-tag (IFNAR1-H10) was produced in Sf9 insect cells using a baculoviral expression system. The cDNA of IFNAR1-H10 without secretion sequence was cloned into the vector pACgp67B and was cotransfected with linearized baculovirus DNA (BaculoGOLD; BD) according to the manufacturer's instructions. After infection of Sf9 cells, the protein was purified from the supernatant by immobilized metal ion affinity chromatography (HiTrap Chelating; GE Healthcare) and by size exclusion chromatography (Superdex 200; GE Healthcare) in HBS buffer (Lamken et al., 2004). IFNAR2-H10 was produced in *E. coli* and purified by anion exchange chromatography (HiTrap Q; GE Healthcare) and size exclusion chromatography (Superdex 75; GE Healthcare) in HBS buffer as described previously (Piehler and Schreiber, 1999a).

### Cell culture, transfection, and live cell labeling

Cells were cultivated at 37°C and 5% CO<sub>2</sub> in minimum essential medium with Earle's salts and stable glutamine (Biochrom AG) supplemented with 10% FBS (Biochrom AG), 1% nonessential amino acids (PAA laboratories GmbH M11003), and 1% 2-[4-(2-hydroxyethyl)-1-piperazineethanesulfonic acid (Hepes) buffer without addition of antibiotics. For minimizing background from nonspecifically adsorbed dye molecules, glass coverslips were coated with a poly-L-lysine (PLL)-graft-(polyethylene glycol) copolymer functionalized with RGD peptide (PLL-PEG-RGD), which was synthesized as described previously in principle (VandeVondele et al., 2003). In brief, 36 mg N-hydroxysuccinimidyl-PEG3000-maleimide (PEG molecular mass: 3,000 g/mol; Rapp Polymere) was mixed with 7.6 mg RGD peptide (Ac-CGRGDS-COOH, custom-synthesized by Coring System Diagnostix) in 0.30 ml HBS buffer (100 mM Hepes buffer with saline, pH 7.5) for 15 min. The reaction solution was immediately added to a solution of 7.5 mg PLL (22.5 kg/mol average molecular mass; Sigma Aldrich) in 0.30 ml HBS buffer. The total 0.6-ml solution was mixed vigorously by shaking for 20 h at room temperature, followed by dialysis against MilliQ water for 48 h using a 10-kD cut-off membrane. After dialysis, the product was lyophilized

into white powder and stored at  $-20^{\circ}\text{C}$ . Before surface coating, cover slides (24 mm  $\varnothing$ , no. 1, VWR International) were cleaned for 15 min using a plasma cleaner (Femto; Diener electronic). 8  $\mu\text{l}$  of 0.4 mg/ml PLL-PEG-RGD in PBS buffer was sandwiched between two plasma-cleaned cover slides for 1 h. The cover slide was washed with MilliQ water and blow-dried with nitrogen gas. After coating, cover slides were directly used for cell culture or stored at  $-20^{\circ}\text{C}$ . Cells were plated on PLL-PEG-RGD-coated cover slides in 35-mm cell culture dishes to a density of  $\sim 40\%$  confluence. Typically, cells were transfected 1 d after seeding via calcium phosphate precipitation as described previously (Muster et al., 2010). After 12 h, cells were washed twice with PBS buffer and media was exchanged. Transiently transfected cells were typically used for ligand binding or colocalization experiments 24 h after transfection.

U5A cells were stably transfected with HaloTag-IFNAR1 and variants of SNAPf-IFNAR2c (full length,  $-\Delta 265$  and  $-\Delta 346$ ) in two steps: U5A cells were transfected by HaloTag-IFNAR1 via G418 selection. Transfected cells were selected for stable neomycin resistance by cultivation in the presence of 800  $\mu\text{g}/\text{ml}$  G418 (EMD Millipore). A cell clone with homogeneous and moderate expression of HaloTag-IFNAR1 was chosen and proliferated. In a second step, SNAPf-IFNAR2c (and truncated versions) was transfected and selected via Puromycin resistance at 0.4  $\mu\text{g}/\text{ml}$  (EMD Millipore). HaloTag- and SNAPf-tagged proteins were simultaneously labeled with 30 nM HaloTag TMR Ligand (HTL-TMR; Promega) and 80 nM of SNAP-Surface 647 (BG-DY647; New England Biolabs, Inc.) at  $37^{\circ}\text{C}$  for 15 min. After labeling, cells were washed five times with prewarmed PBS to remove unreacted dye. Labeling, washing, and subsequent imaging were performed in custom-made incubation chambers with a volume of 500  $\mu\text{l}$ . Homodimerization of MBP-tagged transmembrane proteins was induced by monoclonal antibody against MBP (r 29.6: sc-13564; Santa Cruz Biotechnology, Inc.).

### Single-molecule imaging experiments

Single-molecule imaging experiments were performed by TIRFM with an inverted microscope (IX71; Olympus) equipped with a triple-line total internal reflection illumination condenser (Olympus) and a back-illuminated electron multiplied (EM) CCD camera (iXon DU897D,  $512 \times 512$  pixels; Andor Technology). A 150x magnification objective lens with a numerical aperture of 1.45 (UApochromat 150x/1.45 TIRFM; Olympus) was used for TIRFM.

$\text{DY}^{647}$ IFNs was excited by a 642-nm laser diode (Luxx 642-140; Omicron) at 0.65 mW (power output after passage of the objective), and a 690/70 bandpass filter (Chroma Technology Corp.) was used for detection. Stacks of 300 frames were recorded at 32 ms/frame. For dual-color acquisition,  $\text{TMR}^{\text{HaloTag-IFNAR1}}$  was excited by a 561-nm diode-pumped solid-state laser (CL-561-200; Crystalaser) at 0.95 mW and  $\text{DY}^{647}\text{SNAPf-IFNAR2}$  by a 642-nm laser diode (Luxx 642-140; Omicron) at 0.65 mW. Fluorescence was detected using a spectral image splitter (DualView; Optical Insight) with a 640 DCXR dichroic beam splitter (Chroma Technology Corp.) in combination with the band-pass filter 585/40 (Semrock) for detection of TMR and 690/70 (Chroma Technology Corp) for detection of DY647 projecting each channel onto  $512 \times 256$  pixels (Fig. S2). Stacks of 300 images were acquired with a time resolution of 32 ms/frame.

All experiments were performed at room temperature in medium without phenol red supplemented with an oxygen scavenger and a redox-active photoprotectant (0.5 mg/ml glucose oxidase [Sigma-Aldrich], 0.04 mg/ml catalase [Roche], 5% wt/vol glucose, 1  $\mu\text{M}$  ascorbic acid, and 1  $\mu\text{M}$  methyl viologene) to minimize photobleaching (Vogelsang et al., 2008). For quantitative ligand-binding studies, 2 nM  $\text{DY}^{647}\text{IFN}\alpha 2$  in medium without phenol red was incubated for at least 5 min and kept in the bulk solution during the whole experiment to ensure equilibrium binding. Receptor dimerization was probed in the presence of the respective unlabeled IFN at a concentration of 50 nM after incubating for at least 5 min if not stated otherwise.

### Single-molecule tracking, colocalization, and particle image cross-correlation spectroscopy (PICCS) analysis

Single-molecule localization and single-molecule tracking were performed by using the multiple-target tracing (MTT) algorithm. The positions of individual fluorescence emitters were determined with subpixel precision in a two-step process, which was developed for high-density single-particle tracking (Sergé et al., 2008), as described previously in detail (Appelhans et al., 2012). Initial emitter positions were identified using a pixel-wise statistical test limiting the rate of false-positive detection to  $10^{-6}$  per pixel. These initial positions were refined to subpixel accuracy in a second step by maximum likelihood estimation modeling the microscope's PSF as a 2D Gaussian profile. From the localization data, single-particle tracking was performed, assuming a maximal expected diffusion coefficient of 0.2  $\mu\text{m}^2/\text{s}$ . Step-length distributions were obtained from single-molecule trajectories (5 steps,

$\sim 160$  ms) and decomposed into diffusive subpopulations by a mixture model of Brownian diffusion. Mean diffusion constants were finally determined by the slope in mean square displacement analysis (2–10 steps).

Before colocalization analysis, both imaging channels were aligned with subpixel precision by using a spatial transformation that corrects for translation, rotation, and scaling. To this end, a transformation matrix was calculated based on a calibration measurement with multicolor fluorescent beads (TetraSpeck microspheres, 0.1  $\mu\text{m}$ ; Invitrogen) visible in both spectral channels (cp2form type "affine"; MATLAB release 2009a; The MathWorks Inc.). Immobile molecules were identified by the density-based spatial clustering of applications with noise (DBSCAN) algorithm (Sander et al., 1998), which forms clusters of points based on the premise of density reachability established between neighboring points that satisfy a given critical density. DBSCAN achieves this task by exploiting the high spatio-temporal persistency of immobile signals. To capture this specific feature, the density estimate, an integration over the number of points within a specified radius, is expanded to include the temporal domain. We further introduce nonlinear distance weighting in our density estimate, specifically a Gaussian weighting that possesses two scaling parameters, one for the spatial and one for the temporal domain. The spatial scaling factor is determined by the expected localization precision while the temporal scaling factor is set according to the expected lifetime of the immobile emitter. Thereby, detections from immobile particles are effectively raised above the critical density via the contribution of all detections of the same emitter due to temporal reoccurrence within a small spatial distance (Waichman et al., 2013). For comparison of diffusive behavior and for colocalization analysis, immobile molecules, identified by DBSCAN, were removed from the dataset to increase tracking fidelity.

For single-molecule colocalization analysis, individual molecules detected in the both spectral channels were regarded as colocalized if found in the same frame within a distance threshold radius of 100 nm. In a consecutive step, colocalized particles were subjected to tracking by the MTT algorithm to generate colocalization trajectories. For the colocalization analysis, only trajectories with a minimum of 10 steps ( $\sim 300$  ms) were considered (Ruprecht et al., 2010b). The fraction of colocalization trajectories was then determined as the number of colocalization trajectories with respect to the number of IFNAR trajectories. Typically, the stably transfected cell line U5A IFNAR1+IFNAR2 shows a moderate excess of IFNAR1, so IFNAR2 was regarded as the limiting partner and therefore taken as reference for maximal ternary complex assembly. Receptor dimerization was corrected for the effective degree of labeling (DOL) as determined for HaloTag-SNAPf-IFNAR2c:

$$\frac{\#HS}{\#S} = \text{DOL}_{\text{Halo}} = 0.22 \pm 0.03; \quad \frac{\#HS}{\#H} = \text{DOL}_{\text{SNAPf}} = 0.43 \pm 0.05$$

$$\#H = \text{DOL}_{\text{Halo}} \times [\text{Protein}]$$

$$\#S = \text{DOL}_{\text{SNAPf}} \times [\text{Protein}]$$

$$\#HS = \text{DOL}_{\text{Halo}} \times \text{DOL}_{\text{SNAPf}} \times [\text{Protein}].$$

The shape of the sigmoidal dimerization-affinity relationship was approximated by a Hill function:

$$f(x) = \text{START} + (\text{END} - \text{START}) \times \frac{x^n}{K^n + x^n}.$$

PICCS analysis was performed according to Semrau et al. (2011). The algorithm allows estimating the correlated fraction  $\alpha$  of particles in channel A colocalized with particles in channel B:

$$C_{\text{cum}}(l) = \alpha P_{\text{cum}}(l) + c_{\text{channelB}} \times \pi l^{\dagger}. \quad (1)$$

For randomly distributed particles without a correlated fraction  $\alpha$ ,  $C_{\text{cum}}$  linearly increases with increasing search radius  $l^{\dagger}$ , with a slope given by the density of particles in channel B.

### Quantification of IFNAR1 binding affinities

The relative binding affinities of the IFN $\alpha 2$  mutants toward IFNAR1 were determined by monitoring ligand dissociation kinetics from IFNAR1 and IFNAR2 tethered onto solid-supported membranes by simultaneous total internal reflection fluorescence spectroscopy and reflectance interference

detection in a flow system as described previously in detail (Gavutis et al., 2005, 2006b). All binding experiments were performed in HBS at 25°C. Solid-supported membranes were generated by injection of small unilamellar vesicles, prepared from 250 μM 1,2-dioleoyl-*sn*-glycero-3-phosphocholine containing 2 mol% Tris-nitrilotriacetic acid steroyloctacylamine (Beutel et al., 2014) by sonication, onto a freshly plasma cleaned transducer slide. The membrane was washed sequentially with HBS, 500 mM imidazole in HBS, and 100 mM EDTA in HBS. Finally, 10 mM NiCl<sub>2</sub> in HBS was injected to load the Tris-NTA head groups with Ni<sup>2+</sup>. 25 nM of the deca-histidine-tagged extracellular part of IFNAR1 and IFNAR2 was injected for binding to the solid-supported membrane. After loading the receptors to the membrane, 50 nM <sup>DY647</sup>IFNα2 was injected. Subsequently, the dissociation of <sup>DY647</sup>IFNα2 from the surface was monitored while rinsing for 300 s with HBS buffer at a flow rate of 10 μl/s. After the experiment, all attached proteins were removed by injecting 500 mM imidazole. The subsequent binding assays were performed on the same lipid bilayer.

Relative binding affinities were determined from the ligand dissociation kinetics, which report on the equilibrium between binary and ternary complexes as detailed previously (Gavutis et al., 2005). To this end, the ligand dissociation curve was fitted numerically by a set of differential equations based on a two-step assembly model using Berkeley Madonna software:

$$\frac{d[T]}{dt} = k_a^T \times [B] \times ([R1]_0 - [T]) - k_d^T \times [T]$$

$$\frac{d[B]}{dt} = -k_a^T \times [B] \times ([R1]_0 - [T]) + k_d^T \times [T] - k_b^B \times [B]$$

$$[S] = [T] + [B] \text{ with } [T]_{t=0} = [R2]_0, [B]_{t=0} = 0.$$

[B] and [T] are the surface concentrations of the binary complexes (IFNAR2/IFN) and the ternary complex, respectively. [R1] and [R2] are the surface concentrations of free IFNAR1-H10 and IFNAR2-H10, respectively. [R1]<sub>0</sub> and [R2]<sub>0</sub> are the total surface concentrations of IFNAR1-H10 and IFNAR2-H10, respectively. The 2D association rate constant  $k_a^T$  experimentally assessed for IFNα2 wt (Gavutis et al., 2005) was fixed and the 2D dissociation rate constant  $k_d^T$  was fitted for the IFNα2 mutants, keeping all other parameters constant. The 2D equilibrium dissociation constants  $K_D^T$  were calculated from  $k_a^T$  and  $k_d^T$ . The relative 3D affinity toward IFNAR1 was estimated from the relative  $K_D^T$ , as both affinities are proportional (Gavutis et al., 2006a).

#### Calculation of 2D binding equilibrium constant in cells

The 2D equilibrium dissociation constant of IFNAR1 recruitment into the ternary complex  $K_D^T$  (molecules/μm<sup>2</sup>) was calculated according to the law of mass action:

$$K_D^T = \frac{([IFNAR1] - (\alpha \times [IFNAR2])) \times ([IFNAR2] - (\alpha \times [IFNAR2]))}{(\alpha \times [IFNAR2])}$$

or

$$K_D^T = [IFNAR1] \times \left( \frac{1}{\alpha} - 1 \right) + [IFNAR2] \times (\alpha - 1),$$

where α is the fraction of IFNAR2-bound IFN in ternary complex with IFNAR1 (assuming [IFNAR1] > [IFNAR2]). Receptor cell surface concentrations in stably transfected U5A cells were determined from single particle localizations (molecules/μm<sup>2</sup>) of <sup>TMRE</sup>HaloTag-IFNAR1 (0.78 ± 0.19) and <sup>DY647</sup>SNAPf-IFNAR2c (0.56 ± 0.15). The number of localizations was corrected for the degree of labeling. The degree of labeling was determined as described in the "Single-molecule tracking, colocalization, and particle image crosscorrelation spectroscopy (PICCS) analysis" section, which resulted in effective cell surface concentrations for IFNAR1 (3.5 μm<sup>-2</sup>) and IFNAR2 (1.3 μm<sup>-2</sup>). The correlated fraction α was normalized to the maximum dimerization level (0.89) obtained from the dimerization-affinity relationship.

The calculated  $K_D^T$  was applied to other cell lines with different [IFNAR1/2] to determine α. For HLLR1 and HU13-cells, receptor concentrations were measured by quantitative ligand binding assays:

$$\alpha = \left( 1 + \frac{K_D}{2C} \right) \pm 2 \sqrt{\left( 1 + \frac{K_D}{2C} \right)^2 - 1}.$$

For 0 ≤ α ≤ 1:

$$[IFNAR1] \approx [IFNAR2] = C.$$

The energetic contribution of the intracellular complex stabilization was calculated from the ratio of the equilibrium binding constants:

$$\Delta\Delta G = -RT \ln \left( \frac{5.4}{0.29} \right) = -7.1 \frac{kJ}{mol} \approx 3RT.$$

#### Online supplemental material

Fig. S1 shows binding and diffusion properties of <sup>DY647</sup>IFNα2 mutants to endogenous IFNAR. Fig. S2 shows the specificity of posttranslational labeling of HaloTag-IFNAR1 and SNAPf-IFNAR2 via HTL-TMR and BG-DY647, and includes a schematic flowchart for image acquisition, single-molecule localization, colocalization, and data evaluation. Fig. S3 shows the quantification of receptor dimerization by colocalization and by PICCS. Fig. S4 shows the in vitro quantification of IFNα2 binding affinities toward IFNAR1. Fig. S5 shows the desensitization of IFN signaling in HeLa cells upon priming with IFNα2-M148A. Table S1 summarizes the binding affinities of IFNs used in this study. Table S2 shows the calculation of dimerization fraction α and  $K_D^T$  according to the law of mass action. Table S3 summarizes affinities of IFNs toward IFNAR1 as obtained in vitro. Video 1 shows imaging of individual <sup>DY647</sup>IFNα2 bound to endogenous IFNAR in HeLa cells. Video 2 shows single-step bleaching of <sup>DY647</sup>IFNα2-dn bound to endogenous IFNAR on HeLa. Video 3 shows imaging of <sup>DY647</sup>IFNα2-M148A bound to a HeLa cell transiently overexpressing USP18-EGFP compared with a control cell. Video 4 shows interaction dynamics of <sup>DY647</sup>IFNα2-M148A on HLLR1 and HU13 quantified by single-molecule tracking. Video 5 shows simultaneous dual-color imaging of posttranslationally labeled HaloTag-IFNAR1 and SNAPf-IFNAR2. Video 6 shows negative and positive controls for the colocalization analysis. Video 7 shows colocalization of IFNAR1 and IFNAR2 in the absence and presence of IFNα2. Video 8 shows the single-step bleaching events of two IFN-induced IFNAR1/IFNAR2 dimers. Video 9 shows assembly, colocalization, and dissociation of an individual signaling complex. Online supplemental material is available at <http://www.jcb.org/cgi/content/full/jcb.201412049/DC1>.

We thank Gabriele Hikade and Hella Kenneweg (University of Osnabrück) for technical support, Domenik Lisse (University of Osnabrück) for technical advice concerning HaloTag labeling, Rainer Kurre (Center for Advanced Light Microscopy Osnabrück) for support with fluorescence microscopy, Darren Baker (Biogen Idec) for providing IFNβ, and Ignacio Moraga (Stanford University) for graphic material.

This project was supported by funding from the Deutsche Forschungsgemeinschaft (Sonderforschungsbereich 944) to J. Piehler and by the European Community's Seventh Framework Program (FP7/2007-2013) under grant agreement no. 223608 (IFNaction) to J. Piehler, S. Pellegrini, and G. Uzé. S. Pellegrini was supported by Institut Pasteur, Centre National pour la Recherche Scientifique, and Institut National de la Santé et de la Recherche Médicale. V. Francois-Newton was supported by the Ligue contre le Cancer.

The authors declare no competing financial interests.

Submitted: 10 December 2014

Accepted: 20 April 2015

## References

- Abramovich, C., J. Chebath, and M. Revel. 1994. The human interferon α-receptor protein confers differential responses to human interferon-β versus interferon-α subtypes in mouse and hamster cell transfectants. *Cytokine* 6:414-424. [http://dx.doi.org/10.1016/1043-4666\(94\)90066-3](http://dx.doi.org/10.1016/1043-4666(94)90066-3)
- Appelhans, T., C.P. Richter, V. Wilkens, S.T. Hess, J. Piehler, and K.B. Busch. 2012. Nanoscale organization of mitochondrial microcompartments revealed by combining tracking and localization microscopy. *Nano Lett.* 12:610-616. <http://dx.doi.org/10.1021/nl203343a>
- Beutel, O., J. Nikolaus, O. Birkholz, C. You, T. Schmidt, A. Herrmann, and J. Piehler. 2014. High-fidelity protein targeting into membrane lipid

- microdomains in living cells. *Angew. Chem. Int. Ed. Engl.* 53:1311–1315. <http://dx.doi.org/10.1002/anie.201306328>
- Brooks, A.J., W. Dai, M.L. O'Mara, D. Abankwa, Y. Chhabra, R.A. Pelekanos, O. Gardon, K.A. Tunny, K.M. Blucher, C.J. Morton, et al. 2014. Mechanism of activation of protein kinase JAK2 by the growth hormone receptor. *Science*. 344:1249783. <http://dx.doi.org/10.1126/science.1249783>
- Brown, R.J., J.J. Adams, R.A. Pelekanos, Y. Wan, W.J. McKinstry, K. Palethorpe, R.M. Seeber, T.A. Monks, K.A. Eidne, M.W. Parker, and M.J. Waters. 2005. Model for growth hormone receptor activation based on subunit rotation within a receptor dimer. *Nat. Struct. Mol. Biol.* 12:814–821. <http://dx.doi.org/10.1038/nsmb977>
- Cajean-Feroldi, C., F. Nosal, P.C. Nardeux, X. Gallet, J. Guymarho, F. Baychelier, P. Sempé, M.G. Tovey, J.L. Escary, and P. Eid. 2004. Identification of residues of the IFNAR1 chain of the type I human interferon receptor critical for ligand binding and biological activity. *Biochemistry*. 43:12498–12512. <http://dx.doi.org/10.1021/bi049111r>
- Chill, J.H., S.R. Quadt, R. Levy, G. Schreiber, and J. Anglister. 2003. The human type I interferon receptor: NMR structure reveals the molecular basis of ligand binding. *Structure*. 11:791–802. [http://dx.doi.org/10.1016/S0969-2126\(03\)00120-5](http://dx.doi.org/10.1016/S0969-2126(03)00120-5)
- Coelho, L.F., G. Magno de Freitas Almeida, F.J. Mennechet, A. Blangy, and G. Uzé. 2005. Interferon- $\alpha$  and - $\beta$  differentially regulate osteoclastogenesis: role of differential induction of chemokine CXCL11 expression. *Proc. Natl. Acad. Sci. USA*. 102:11917–11922. <http://dx.doi.org/10.1073/pnas.0502188102>
- Cohen, B., D. Novick, S. Barak, and M. Rubinstein. 1995. Ligand-induced association of the type I interferon receptor components. *Mol. Cell. Biol.* 15:4208–4214.
- Constantinescu, S.N., T. Keren, M. Socolovsky, H. Nam, Y.I. Henis, and H.F. Lodish. 2001. Ligand-independent oligomerization of cell-surface erythropoietin receptor is mediated by the transmembrane domain. *Proc. Natl. Acad. Sci. USA*. 98:4379–4384. <http://dx.doi.org/10.1073/pnas.081069198>
- Damjanovich, S., L. Bene, J. Matkó, A. Alileche, C.K. Goldman, S. Sharrow, and T.A. Waldmann. 1997. Preassembly of interleukin 2 (IL-2) receptor subunits on resting Kit 225 K6 T cells and their modulation by IL-2, IL-7, and IL-15: a fluorescence resonance energy transfer study. *Proc. Natl. Acad. Sci. USA*. 94:13134–13139. <http://dx.doi.org/10.1073/pnas.94.24.13134>
- de Bakker, B.I., A. Bodnár, E.M. van Dijk, G. Vámosi, S. Damjanovich, T.A. Waldmann, N.F. van Hulst, A. Jenéi, and M.F. Garcia-Parajo. 2008. Nanometer-scale organization of the alpha subunits of the receptors for IL2 and IL15 in human T lymphoma cells. *J. Cell Sci.* 121:627–633. <http://dx.doi.org/10.1242/jcs.019513>
- Decker, T., M. Müller, and S. Stockinger. 2005. The yin and yang of type I interferon activity in bacterial infection. *Nat. Rev. Immunol.* 5:675–687. <http://dx.doi.org/10.1038/nri1684>
- Deonarain, R., D.C. Chan, L.C. Platanias, and E.N. Fish. 2002. Interferon- $\alpha$ / $\beta$ -receptor interactions: a complex story unfolding. *Curr. Pharm. Des.* 8:2131–2137. <http://dx.doi.org/10.2174/1381612023393288>
- de Weerd, N.A., J.P. Vivian, T.K. Nguyen, N.E. Mangan, J.A. Gould, S.J. Braniff, L. Zaker-Tabrizi, K.Y. Fung, S.C. Forster, T. Beddoe, et al. 2013. Structural basis of a unique interferon- $\beta$  signaling axis mediated via the receptor IFNAR1. *Nat. Immunol.* 14:901–907. <http://dx.doi.org/10.1038/ni.2667>
- Domanski, P., O.W. Nadeau, L.C. Platanias, E. Fish, M. Kellum, P. Pitha, and O.R. Colamonici. 1998. Differential use of the  $\beta$ L subunit of the type I interferon (IFN) receptor determines signaling specificity for IFN $\alpha$ 2 and IFN $\beta$ . *J. Biol. Chem.* 273:3144–3147. <http://dx.doi.org/10.1074/jbc.273.6.3144>
- Dunne, P.D., R.A. Fernandes, J. McColl, J.W. Yoon, J.R. James, S.J. Davis, and D. Klenerman. 2009. DySCO: quantitating associations of membrane proteins using two-color single-molecule tracking. *Biophys. J.* 97:L5–L7. <http://dx.doi.org/10.1016/j.bpj.2009.05.046>
- François-Newton, V., G. Magno de Freitas Almeida, B. Payelle-Brogard, D. Monneron, L. Pichard-Garcia, J. Piehler, S. Pellegrini, and G. Uzé. 2011. USP18-based negative feedback control is induced by type I and type III interferons and specifically inactivates interferon  $\alpha$  response. *PLoS ONE*. 6:e22200. <http://dx.doi.org/10.1371/journal.pone.0022200>
- François-Newton, V., M. Livingstone, B. Payelle-Brogard, G. Uzé, and S. Pellegrini. 2012. USP18 establishes the transcriptional and anti-proliferative interferon  $\alpha/\beta$  differential. *Biochem. J.* 446:509–516. <http://dx.doi.org/10.1042/BJ20120541>
- Gavutis, M., S. Lata, P. Lamken, P. Müller, and J. Piehler. 2005. Lateral ligand-receptor interactions on membranes probed by simultaneous fluorescence-interference detection. *Biophys. J.* 88:4289–4302. <http://dx.doi.org/10.1529/biophysj.104.055855>
- Gavutis, M., E. Jaks, P. Lamken, and J. Piehler. 2006a. Determination of the two-dimensional interaction rate constants of a cytokine receptor complex. *Biophys. J.* 90:3345–3355. <http://dx.doi.org/10.1529/biophysj.105.072546>
- Gavutis, M., S. Lata, and J. Piehler. 2006b. Probing 2-dimensional protein-protein interactions on model membranes. *Nat. Protoc.* 1:2091–2103. <http://dx.doi.org/10.1038/nprot.2006.270>
- Hertzog, P.J., and B.R. Williams. 2013. Fine tuning type I interferon responses. *Cytokine Growth Factor Rev.* 24:217–225. <http://dx.doi.org/10.1016/j.cytogfr.2013.04.002>
- Jaitin, D.A., L.C. Roisman, E. Jaks, M. Gavutis, J. Piehler, J. Van der Heyden, G. Uze, and G. Schreiber. 2006. Inquiring into the differential action of interferons (IFNs): an IFN- $\alpha$ 2 mutant with enhanced affinity to IFNAR1 is functionally similar to IFN- $\beta$ . *Mol. Cell. Biol.* 26:1888–1897. <http://dx.doi.org/10.1128/MCB.26.5.1888-1897.2006>
- Jaks, E., M. Gavutis, G. Uzé, J. Martal, and J. Piehler. 2007. Differential receptor subunit affinities of type I interferons govern differential signal activation. *J. Mol. Biol.* 366:525–539. <http://dx.doi.org/10.1016/j.jmb.2006.11.053>
- Jenéi, A., J. Kormos, G. Szentesi, A.J. Veres, S. Varga, A. Bodnár, S. Damjanovich, and L. Mátyus. 2009. Non-random distribution of interleukin receptors on the cell surface. *ChemPhysChem*. 10:1577–1585. <http://dx.doi.org/10.1002/cphc.200900242>
- Junttila, I.S., R.J. Creusot, I. Moraga, D.L. Bates, M.T. Wong, M.N. Alonso, M.M. Suhoski, P. Lupardus, M. Meier-Schellersheim, E.G. Engleman, et al. 2012. Redirecting cell-type specific cytokine responses with engineered interleukin-4 superkines. *Nat. Chem. Biol.* 8:990–998. <http://dx.doi.org/10.1038/nchembio.1096>
- Kalie, E., D.A. Jaitin, R. Abramovich, and G. Schreiber. 2007. An interferon  $\alpha$ 2 mutant optimized by phage display for IFNAR1 binding confers specifically enhanced antitumor activities. *J. Biol. Chem.* 282:11602–11611. <http://dx.doi.org/10.1074/jbc.M610115200>
- Koyama-Honda, I., K. Ritchie, T. Fujiwara, R. Iino, H. Murakoshi, R.S. Kasai, and A. Kusumi. 2005. Fluorescence imaging for monitoring the colocalization of two single molecules in living cells. *Biophys. J.* 88:2126–2136. <http://dx.doi.org/10.1529/biophysj.104.048967>
- Krause, C.D., E. Mei, J. Xie, Y. Jia, M.A. Bopp, R.M. Hochstrasser, and S. Pestka. 2002. Seeing the light: preassembly and ligand-induced changes of the interferon gamma receptor complex in cells. *Mol. Cell. Proteomics*. 1:805–815. <http://dx.doi.org/10.1074/mcp.M200065-MCP200>
- Krause, C.D., N. Lavnikova, J. Xie, E. Mei, O.V. Mirochnitchenko, Y. Jia, R.M. Hochstrasser, and S. Pestka. 2006a. Preassembly and ligand-induced restructuring of the chains of the IFN- $\gamma$  receptor complex: the roles of Jak kinases, Stat1 and the receptor chains. *Cell Res.* 16:55–69. <http://dx.doi.org/10.1038/sj.cr.7310008>
- Krause, C.D., E. Mei, O. Mirochnitchenko, N. Lavnikova, J. Xie, Y. Jia, R.M. Hochstrasser, and S. Pestka. 2006b. Interactions among the components of the interleukin-10 receptor complex. *Biochem. Biophys. Res. Commun.* 340:377–385. <http://dx.doi.org/10.1016/j.bbrc.2005.11.182>
- Krause, C.D., G. Digioia, L.S. Izotova, J. Xie, Y. Kim, B.J. Schwartz, O.V. Mirochnitchenko, and S. Pestka. 2013. Ligand-independent interaction of the type I interferon receptor complex is necessary to observe its biological activity. *Cytokine*. 64:286–297. <http://dx.doi.org/10.1016/j.cyto.2013.06.309>
- Kusumi, A., T.K. Fujiwara, R. Chadda, M. Xie, T.A. Tsunoyama, Z. Kalay, R.S. Kasai, and K.G. Suzuki. 2012. Dynamic organizing principles of the plasma membrane that regulate signal transduction: commemorating the fortieth anniversary of Singer and Nicolson's fluid-mosaic model. *Annu. Rev. Cell Dev. Biol.* 28:215–250. <http://dx.doi.org/10.1146/annurev-cellbio-100809-151736>
- Lamken, P., S. Lata, M. Gavutis, and J. Piehler. 2004. Ligand-induced assembling of the type I interferon receptor on supported lipid bilayers. *J. Mol. Biol.* 341:303–318. <http://dx.doi.org/10.1016/j.jmb.2004.05.059>
- Lamken, P., M. Gavutis, I. Peters, J. Van der Heyden, G. Uzé, and J. Piehler. 2005. Functional cartography of the ectodomain of the type I interferon receptor subunit ifnar1. *J. Mol. Biol.* 350:476–488. <http://dx.doi.org/10.1016/j.jmb.2005.05.008>
- LaPorte, S.L., Z.S. Juo, J. Vaclavikova, L.A. Colf, X. Qi, N.M. Heller, A.D. Keegan, and K.C. Garcia. 2008. Molecular and structural basis of cytokine receptor pleiotropy in the interleukin-4/13 system. *Cell*. 132:259–272. <http://dx.doi.org/10.1016/j.cell.2007.12.030>
- Lavoie, T.B., E. Kalie, S. Crisafulli-Cabatu, R. Abramovich, G. DiGioia, K. Moolchan, S. Pestka, and G. Schreiber. 2011. Binding and activity of all human alpha interferon subtypes. *Cytokine*. 56:282–289. <http://dx.doi.org/10.1016/j.cyto.2011.07.019>
- Levin, D., D. Harari, and G. Schreiber. 2011. Stochastic receptor expression determines cell fate upon interferon treatment. *Mol. Cell. Biol.* 31:3252–3266. <http://dx.doi.org/10.1128/MCB.05251-11>
- Levin, D., W.M. Schneider, H.H. Hoffmann, G. Yarden, A.G. Busetto, O. Manor, N. Sharma, C.M. Rice, and G. Schreiber. 2014. Multifaceted activities of

- type I interferon are revealed by a receptor antagonist. *Sci. Signal.* 7:ra50. <http://dx.doi.org/10.1126/scisignal.2004998>
- Li, Z., J.J. Strunk, P. Lamken, J. Piehler, and T. Walz. 2008. The EM structure of a type I interferon-receptor complex reveals a novel mechanism for cytokine signaling. *J. Mol. Biol.* 377:715–724. <http://dx.doi.org/10.1016/j.jmb.2007.12.005>
- Löchte, S., S. Waichman, O. Beutel, C. You, and J. Piehler. 2014. Live cell micropatterning reveals the dynamics of signaling complexes at the plasma membrane. *J. Cell Biol.* 207:407–418. <http://dx.doi.org/10.1083/jcb.201406032>
- Low-Nam, S.T., K.A. Lidke, P.J. Cutler, R.C. Roovers, P.M. van Bergen en Henegouwen, B.S. Wilson, and D.S. Lidke. 2011. ErbB1 dimerization is promoted by domain co-confinement and stabilized by ligand binding. *Nat. Struct. Mol. Biol.* 18:1244–1249. <http://dx.doi.org/10.1038/nsmb.2135>
- Malakhova, O.A., K.I. Kim, J.K. Luo, W. Zou, K.G. Kumar, S.Y. Fuchs, K. Shuai, and D.E. Zhang. 2006. UBP43 is a novel regulator of interferon signaling independent of its ISG15 isopeptidase activity. *EMBO J.* 25:2358–2367. <http://dx.doi.org/10.1038/sj.emboj.7601149>
- Marchetti, M., M.N. Monier, A. Fradagrada, K. Mitchell, F. Baychelier, P. Eid, L. Johannes, and C. Lamaze. 2006. Stat-mediated signaling induced by type I and type II interferons (IFNs) is differentially controlled through lipid microdomain association and clathrin-dependent endocytosis of IFN receptors. *Mol. Biol. Cell.* 17:2896–2909. <http://dx.doi.org/10.1091/mbc.E06-01-0076>
- Moraga, I., D. Harari, G. Schreiber, G. Uzé, and S. Pellegrini. 2009. Receptor density is key to the  $\alpha 2/\beta$  interferon differential activities. *Mol. Cell Biol.* 29:4778–4787. <http://dx.doi.org/10.1128/MCB.01808-08>
- Moraga, I., J. Spangler, J.L. Mendoza, and K.C. Garcia. 2014. Multifarious determinants of cytokine receptor signaling specificity. *Adv. Immunol.* 121:1–39. <http://dx.doi.org/10.1016/B978-0-12-800100-4.00001-5>
- Muster, B., W. Kohl, I. Wittig, V. Strecker, F. Joos, W. Haase, J. Bereiter-Hahn, and K. Busch. 2010. Respiratory chain complexes in dynamic mitochondria display a patchy distribution in life cells. *PLoS ONE.* 5:e11910. <http://dx.doi.org/10.1371/journal.pone.0011910>
- Novick, D., B. Cohen, and M. Rubinstein. 1994. The human interferon  $\alpha/\beta$  receptor: characterization and molecular cloning. *Cell.* 77:391–400. [http://dx.doi.org/10.1016/0092-8674\(94\)90154-6](http://dx.doi.org/10.1016/0092-8674(94)90154-6)
- Pan, M., E. Kalie, B.J. Scaglione, E.S. Raveche, G. Schreiber, and J.A. Langer. 2008. Mutation of the IFNAR-1 receptor binding site of human IFN- $\alpha 2$  generates type I IFN competitive antagonists. *Biochemistry.* 47:12018–12027. <http://dx.doi.org/10.1021/bi801588g>
- Parmar, S., and L.C. Platanias. 2003. Interferons: mechanisms of action and clinical applications. *Curr. Opin. Oncol.* 15:431–439. <http://dx.doi.org/10.1097/00001622-200311000-00005>
- Pestka, S., C.D. Krause, and M.R. Walter. 2004. Interferons, interferon-like cytokines, and their receptors. *Immunol. Rev.* 202:8–32. <http://dx.doi.org/10.1111/j.0105-2896.2004.00204.x>
- Piebler, J., and G. Schreiber. 1999a. Biophysical analysis of the interaction of human ifnar2 expressed in *E. coli* with IFN $\alpha 2$ . *J. Mol. Biol.* 289:57–67. <http://dx.doi.org/10.1006/jmbi.1999.2726>
- Piebler, J., and G. Schreiber. 1999b. Mutational and structural analysis of the binding interface between type I interferons and their receptor Ifnar2. *J. Mol. Biol.* 294:223–237. <http://dx.doi.org/10.1006/jmbi.1999.3230>
- Piebler, J., L.C. Roisman, and G. Schreiber. 2000. New structural and functional aspects of the type I interferon-receptor interaction revealed by comprehensive mutational analysis of the binding interface. *J. Biol. Chem.* 275:40425–40433. <http://dx.doi.org/10.1074/jbc.M006854200>
- Piebler, J., C. Thomas, K.C. Garcia, and G. Schreiber. 2012. Structural and dynamic determinants of type I interferon receptor assembly and their functional interpretation. *Immunol. Rev.* 250:317–334. <http://dx.doi.org/10.1111/imr.12001>
- Quadt-Akabayov, S.R., J.H. Chill, R. Levy, N. Kessler, and J. Anglister. 2006. Determination of the human type I interferon receptor binding site on human interferon- $\alpha 2$  by cross saturation and an NMR-based model of the complex. *Protein Sci.* 15:2656–2668. <http://dx.doi.org/10.1110/ps.062283006>
- Rani, M.R., G.R. Foster, S. Leung, D. Leaman, G.R. Stark, and R.M. Ransohoff. 1996. Characterization of  $\beta$ -R1, a gene that is selectively induced by interferon  $\beta$  (IFN- $\beta$ ) compared with IFN- $\alpha$ . *J. Biol. Chem.* 271:22878–22884. <http://dx.doi.org/10.1074/jbc.271.37.22878>
- Remy, I., I.A. Wilson, and S.W. Michnick. 1999. Erythropoietin receptor activation by a ligand-induced conformation change. *Science.* 283:990–993. <http://dx.doi.org/10.1126/science.283.5404.990>
- Ring, A.M., J.X. Lin, D. Feng, S. Mitra, M. Rickert, G.R. Bowman, V.S. Pande, P. Li, I. Moraga, R. Spolski, et al. 2012. Mechanistic and structural insight into the functional dichotomy between IL-2 and IL-15. *Nat. Immunol.* 13:1187–1195. <http://dx.doi.org/10.1038/ni.2449>
- Roder, F., S. Wilmes, C.P. Richter, and J. Piehler. 2014. Rapid transfer of transmembrane proteins for single molecule dimerization assays in polymer-supported membranes. *ACS Chem. Biol.* 9:2479–2484. <http://dx.doi.org/10.1021/cb5005806>
- Roisman, L.C., J. Piehler, J.Y. Trosset, H.A. Scheraga, and G. Schreiber. 2001. Structure of the interferon-receptor complex determined by distance constraints from double-mutant cycles and flexible docking. *Proc. Natl. Acad. Sci. USA.* 98:13231–13236. <http://dx.doi.org/10.1073/pnas.221290398>
- Roisman, L.C., D.A. Jaitin, D.P. Baker, and G. Schreiber. 2005. Mutational analysis of the IFNAR1 binding site on IFN $\alpha 2$  reveals the architecture of a weak ligand-receptor binding-site. *J. Mol. Biol.* 353:271–281. <http://dx.doi.org/10.1016/j.jmb.2005.08.042>
- Runkel, L., C. deDios, M. Karpusas, M. Betzenhauser, C. Muldowney, M. Zafari, C.D. Benjamin, S. Miller, P.S. Hochman, and A. Whitty. 2000. Systematic mutational mapping of sites on human interferon- $\beta$ -1a that are important for receptor binding and functional activity. *Biochemistry.* 39:2538–2551. <http://dx.doi.org/10.1021/bi991631c>
- Ruprecht, V., M. Brameshuber, and G.J. Schutz. 2010a. Two-color single molecule tracking combined with photobleaching for the detection of rare molecular interactions in fluid biomembranes. *Soft Matter.* 6:568–581. <http://dx.doi.org/10.1039/B916734J>
- Ruprecht, V., J. Weghuber, S. Wieser, and G.J. Schütz. 2010b. Measuring colocalization by dual color single molecule imaging: Thresholds, error rates, and sensitivity. *Advances in Planar Lipid Bilayers and Liposomes.* 12:21–40. <http://dx.doi.org/10.1016/B978-0-12-381266-7.00002-X>
- Russell-Harde, D., T.C. Wagner, H.D. Perez, and E. Croze. 1999. Formation of a uniquely stable type I interferon receptor complex by interferon  $\beta$  is dependent upon particular interactions between interferon  $\beta$  and its receptor and independent of tyrosine phosphorylation. *Biochem. Biophys. Res. Commun.* 255:539–544. <http://dx.doi.org/10.1006/bbrc.1998.0105>
- Sander, J., M. Ester, H.P. Kriegel, and X.W. Xu. 1998. Density-based clustering in spatial databases: The algorithm GDBSCAN and its applications. *Data Min. Knowl. Discov.* 2:169–194. <http://dx.doi.org/10.1023/A:1009745219419>
- Schneider, W.M., M.D. Chevillotte, and C.M. Rice. 2014. Interferon-stimulated genes: a complex web of host defenses. *Annu. Rev. Immunol.* 32:513–545. <http://dx.doi.org/10.1146/annurev-immunol-032713-120231>
- Schreiber, G., and M.R. Walter. 2010. Cytokine-receptor interactions as drug targets. *Curr. Opin. Chem. Biol.* 14:511–519. <http://dx.doi.org/10.1016/j.cbpa.2010.06.165>
- Schütz, G.J., W. Trabesinger, and T. Schmidt. 1998. Direct observation of ligand colocalization on individual receptor molecules. *Biophys. J.* 74:2223–2226. [http://dx.doi.org/10.1016/S0006-3495\(98\)77931-7](http://dx.doi.org/10.1016/S0006-3495(98)77931-7)
- Semrau, S., L. Holtzer, M. González-Gaitán, and T. Schmidt. 2011. Quantification of biological interactions with particle image cross-correlation spectroscopy (PICCS). *Biophys. J.* 100:1810–1818. <http://dx.doi.org/10.1016/j.bpj.2010.12.3746>
- Sergé, A., N. Bertaux, H. Rigneault, and D. Marguet. 2008. Dynamic multiple-target tracing to probe spatiotemporal cartography of cell membranes. *Nat. Methods.* 5:687–694. <http://dx.doi.org/10.1038/nmeth.1233>
- Shimozono, S., and A. Miyawaki. 2008. Engineering FRET constructs using CFP and YFP. *Methods Cell Biol.* 85:381–393. [http://dx.doi.org/10.1016/S0091-679X\(08\)85016-9](http://dx.doi.org/10.1016/S0091-679X(08)85016-9)
- Strunk, J.J., I. Gregor, Y. Becker, Z. Li, M. Gavutis, E. Jaks, P. Lamken, T. Walz, J. Enderlein, and J. Piehler. 2008. Ligand binding induces a conformational change in ifnar1 that is propagated to its membrane-proximal domain. *J. Mol. Biol.* 377:725–739. <http://dx.doi.org/10.1016/j.jmb.2008.01.017>
- Subramaniam, P.S., S.A. Khan, C.H. Pontzer, and H.M. Johnson. 1995. Differential recognition of the type I interferon receptor by interferons tau and alpha is responsible for their disparate cytotoxicities. *Proc. Natl. Acad. Sci. USA.* 92:12270–12274. <http://dx.doi.org/10.1073/pnas.92.26.12270>
- Suzuki, K.G., T.K. Fujiwara, M. Edidin, and A. Kusumi. 2007. Dynamic recruitment of phospholipase C $\gamma$  at transiently immobilized GPI-anchored receptor clusters induces IP $_3$ -Ca $^{2+}$  signaling: single-molecule tracking study 2. *J. Cell Biol.* 177:731–742. <http://dx.doi.org/10.1083/jcb.200609175>
- Suzuki, K.G., R.S. Kasai, K.M. Hirose, Y.L. Nemoto, M. Ishibashi, Y. Miwa, T.K. Fujiwara, and A. Kusumi. 2012. Transient GPI-anchored protein homodimers are units for raft organization and function. *Nat. Chem. Biol.* 8:774–783. <http://dx.doi.org/10.1038/nchembio.1028>
- Tenhuberg, S., B. Schuster, L. Zhu, M. Kovaleva, J. Scheller, K.J. Kallen, and S. Rose-John. 2006. gp130 dimerization in the absence of ligand: preformed cytokine receptor complexes. *Biochem. Biophys. Res. Commun.* 346:649–657. <http://dx.doi.org/10.1016/j.bbrc.2006.05.173>
- Thomas, C., I. Moraga, D. Levin, P.O. Krutzik, Y. Podoplelova, A. Trejo, C. Lee, G. Yarden, S.E. Vleck, J.S. Glenn, et al. 2011. Structural linkage

- between ligand discrimination and receptor activation by type I interferons. *Cell*. 146:621–632. <http://dx.doi.org/10.1016/j.cell.2011.06.048>
- Uzé, G., G. Lutfalla, M.T. Bandu, D. Proud'hon, and K.E. Mogensen. 1992. Behavior of a cloned murine interferon  $\alpha/\beta$  receptor expressed in homo-specific or heterospecific background. *Proc. Natl. Acad. Sci. USA*. 89: 4774–4778. <http://dx.doi.org/10.1073/pnas.89.10.4774>
- Uzé, G., G. Schreiber, J. Piehler, and S. Pellegrini. 2007. The receptor of the type I interferon family. *Curr. Top. Microbiol. Immunol.* 316:71–95.
- Vámosi, G., A. Bodnár, G. Vereb, A. Jenéi, C.K. Goldman, J. Langowski, K. Tóth, L. Mátyus, J. Szöllösi, T.A. Waldmann, and S. Damjanovich. 2004. IL-2 and IL-15 receptor  $\alpha$ -subunits are coexpressed in a supramolecular receptor cluster in lipid rafts of T cells. *Proc. Natl. Acad. Sci. USA*. 101:11082–11087. <http://dx.doi.org/10.1073/pnas.0403916101>
- VandeVondele, S., J. Voros, and J.A. Hubbell. 2003. RGD-grafted poly-L-lysine-graft-(polyethylene glycol) copolymers block non-specific protein adsorption while promoting cell adhesion. *Biotechnol. Bioeng.* 82:784–790. <http://dx.doi.org/10.1002/bit.10625>
- Vogelsang, J., R. Kasper, C. Steinhauer, B. Person, M. Heilemann, M. Sauer, and P. Tinnefeld. 2008. A reducing and oxidizing system minimizes photobleaching and blinking of fluorescent dyes. *Angew. Chem. Int. Ed. Engl.* 47:5465–5469. <http://dx.doi.org/10.1002/anie.200801518>
- Waichman, S., M. Bhagawati, Y. Podoplelova, A. Reichel, A. Brunk, D. Paterok, and J. Piehler. 2010. Functional immobilization and patterning of proteins by an enzymatic transfer reaction. *Anal. Chem.* 82:1478–1485. <http://dx.doi.org/10.1021/ac902608a>
- Waichman, S., F. Roder, C.P. Richter, O. Birkholz, and J. Piehler. 2013. Diffusion and interaction dynamics of individual membrane protein complexes confined in micropatterned polymer-supported membranes. *Small*. 9:570–577. <http://dx.doi.org/10.1002/sml.201201530>
- Whitty, A., N. Raskin, D.L. Olson, C.W. Borysenko, C.M. Ambrose, C.D. Benjamin, and L.C. Burkly. 1998. Interaction affinity between cytokine receptor components on the cell surface. *Proc. Natl. Acad. Sci. USA*. 95:13165–13170. <http://dx.doi.org/10.1073/pnas.95.22.13165>
- Yang, N., X. Wang, J. Jiang, and S.J. Frank. 2007. Role of the growth hormone (GH) receptor transmembrane domain in receptor predimerization and GH-induced activation. *Mol. Endocrinol.* 21:1642–1655. <http://dx.doi.org/10.1210/me.2006-0458>
- Yin, J., P.D. Straight, S.M. McLoughlin, Z. Zhou, A.J. Lin, D.E. Golan, N.L. Kelleher, R. Kolter, and C.T. Walsh. 2005. Genetically encoded short peptide tag for versatile protein labeling by Sfp phosphopantetheinyl transferase. *Proc. Natl. Acad. Sci. USA*. 102:15815–15820. <http://dx.doi.org/10.1073/pnas.0507705102>
- Yoon, S.I., B.C. Jones, N.J. Logsdon, and M.R. Walter. 2005. Same structure, different function crystal structure of the Epstein-Barr virus IL-10 bound to the soluble IL-10R1 chain. *Structure*. 13:551–564. <http://dx.doi.org/10.1016/j.str.2005.01.016>
- Yoon, S.I., B.C. Jones, N.J. Logsdon, B.D. Harris, S. Kuruganti, and M.R. Walter. 2012. Epstein-Barr virus IL-10 engages IL-10R1 by a two-step mechanism leading to altered signaling properties. *J. Biol. Chem.* 287:26586–26595. <http://dx.doi.org/10.1074/jbc.M112.376707>
- Zaks-Zilberman, M., A.E. Harrington, T. Ishino, and I.M. Chaiken. 2008. Interleukin-5 receptor subunit oligomerization and rearrangement revealed by fluorescence resonance energy transfer imaging. *J. Biol. Chem.* 283:13398–13406. <http://dx.doi.org/10.1074/jbc.M710230200>
- Zhang, X., J. Gureasko, K. Shen, P.A. Cole, and J. Kuriyan. 2006. An allosteric mechanism for activation of the kinase domain of epidermal growth factor receptor. *Cell*. 125:1137–1149. <http://dx.doi.org/10.1016/j.cell.2006.05.013>